Vniversitat de València
Generalitat Valenciana
Ministerio de Ciencia, Innovación y Universidades
Funded by the European Union NextGenerationEU
Max-Planck-Institut für Radioastronomie

γ 2024
8th Heidelberg International Symposium on High Energy Gamma Ray Astronomy
Milano, 2-6 September 2024

Deceleration of FR I jet: elucidating the radio-optical shifts

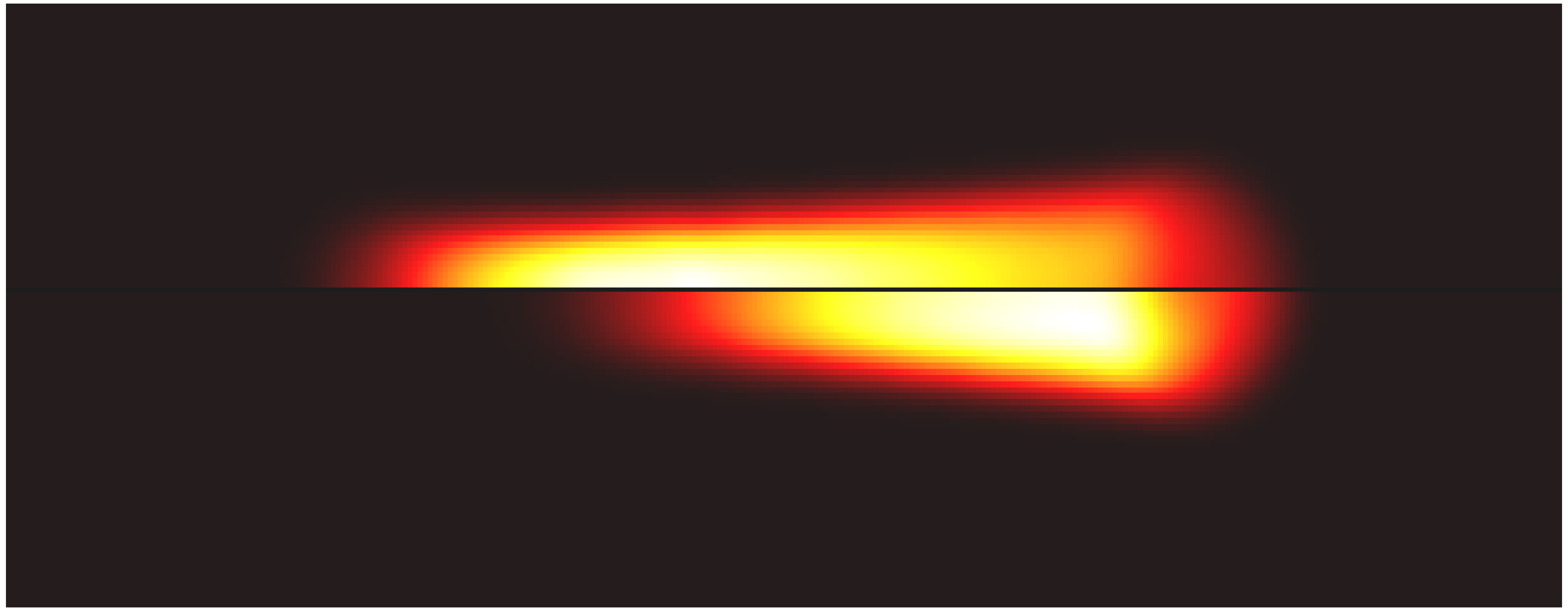

Gaëtan Fichet de Clairfontaine* in collaboration with Manel Perucho, José-María Martí and Yuri Kovalev.

***gaetan.fichet@uv.es**

3rd Sept. 2024

Radio-galaxies: the Fanaroff-Riley classification

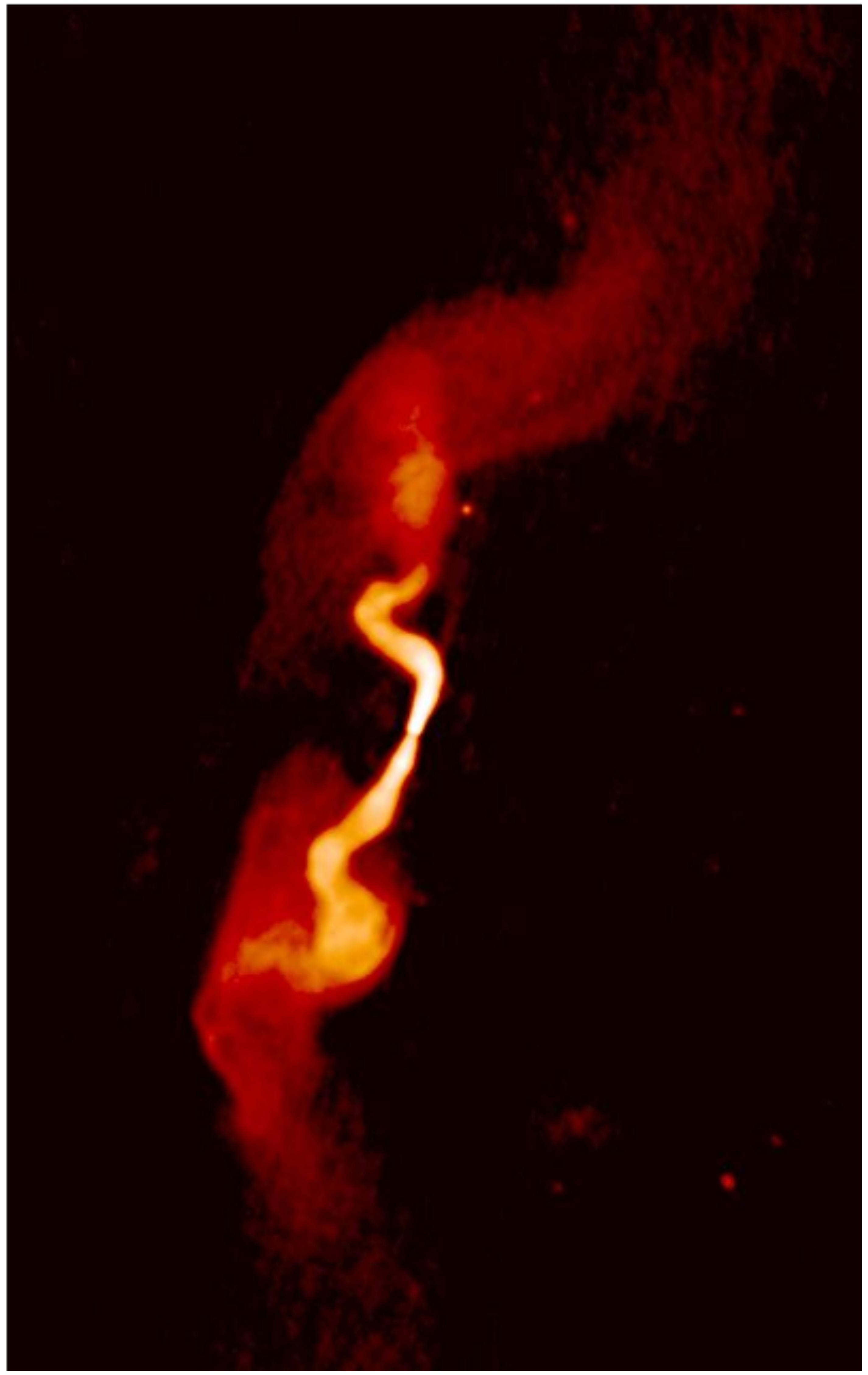

3C 31, FR II, NRAO

What we can observe:

FR I: low-power jets $10^{43-44}\ \mathrm{erg \cdot s^{-1}}$, continuous radio emission, disrupts at the kpc scales in a rich environment.

FR II: high power jets, localized emission (knots, lobes), remains relativistic until the hotspot in a poor environment.

If useful, the FR classification does not offer a satisfying physical scenario that helps to understand the morphological and multi-wavelength characteristics of radio-galaxies.

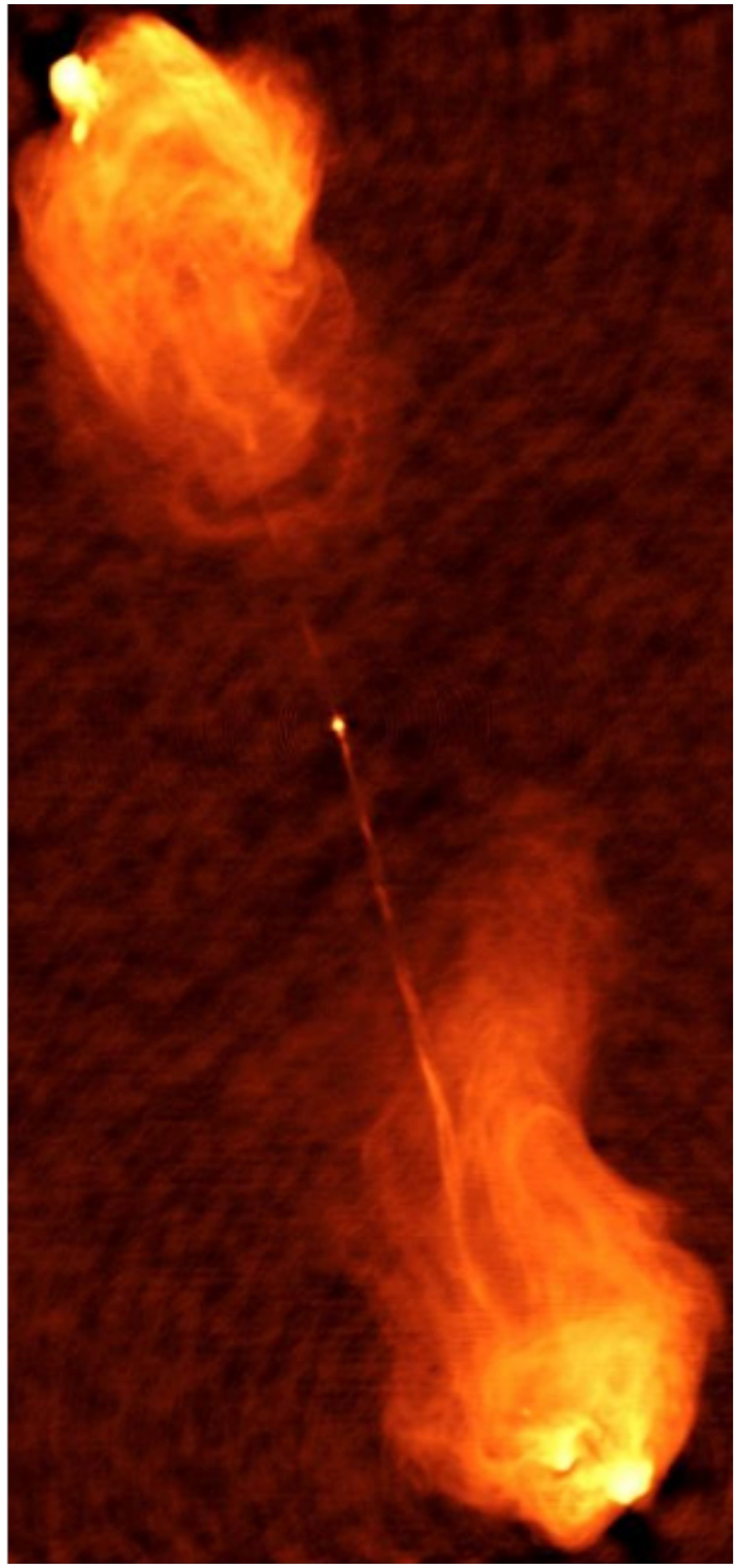

Cygnus A, FR I, NRAO.

A promising scenario: energy dissipation by mass-loading

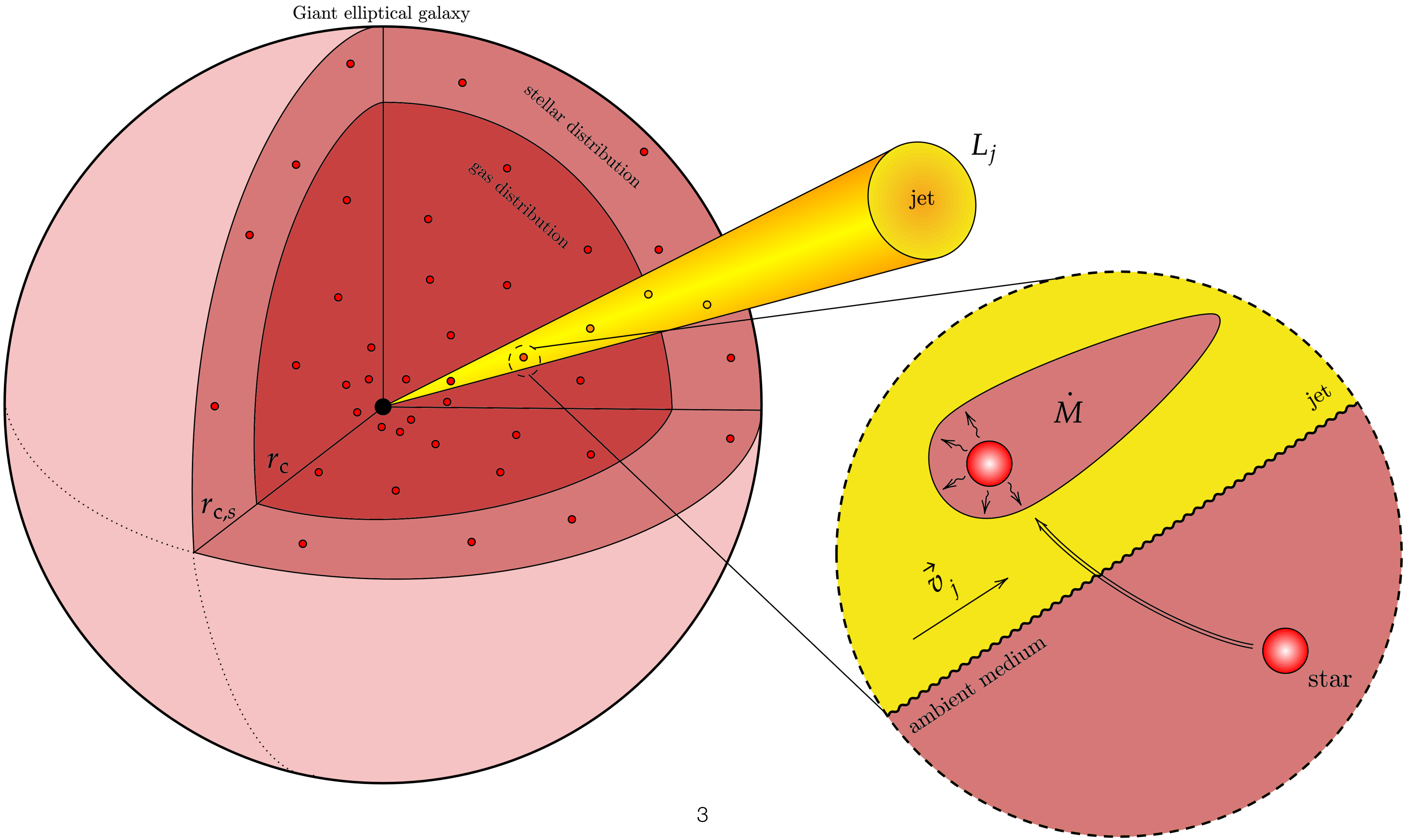

A promising scenario: energy dissipation by mass-loading

Based on the work by Anglés-Castillo, Perucho et al. 2021:

- Simulations of 2000 pc long jets from quasi-1D simulations (Komissarov et al. 2015) with $L_{\mathrm{k,jet}} = 10^{43}\ \mathrm{erg}\cdot\mathrm{s}^{-1}$.
- Pair plasma jets with mean stellar mass-losses ranging from 2×10^{-12} to $10^{-9}\ \mathrm{M}_{\odot}\cdot\mathrm{yr}^{-1}$, for different gas of stellar distribution $(r_{\mathrm{c}}, r_{\mathrm{c,s}})$ that can range from 0.5 to 1.5 kpc.
- Increase of the thermal energy at long distance from the jet base (Bowman et al. 1996), and dilution of e^-, e^+ from mass-loading of protons.
- Large enough mass loading causes jet expansion and deceleration: **promising scenario for radio-galaxy morphologies.**

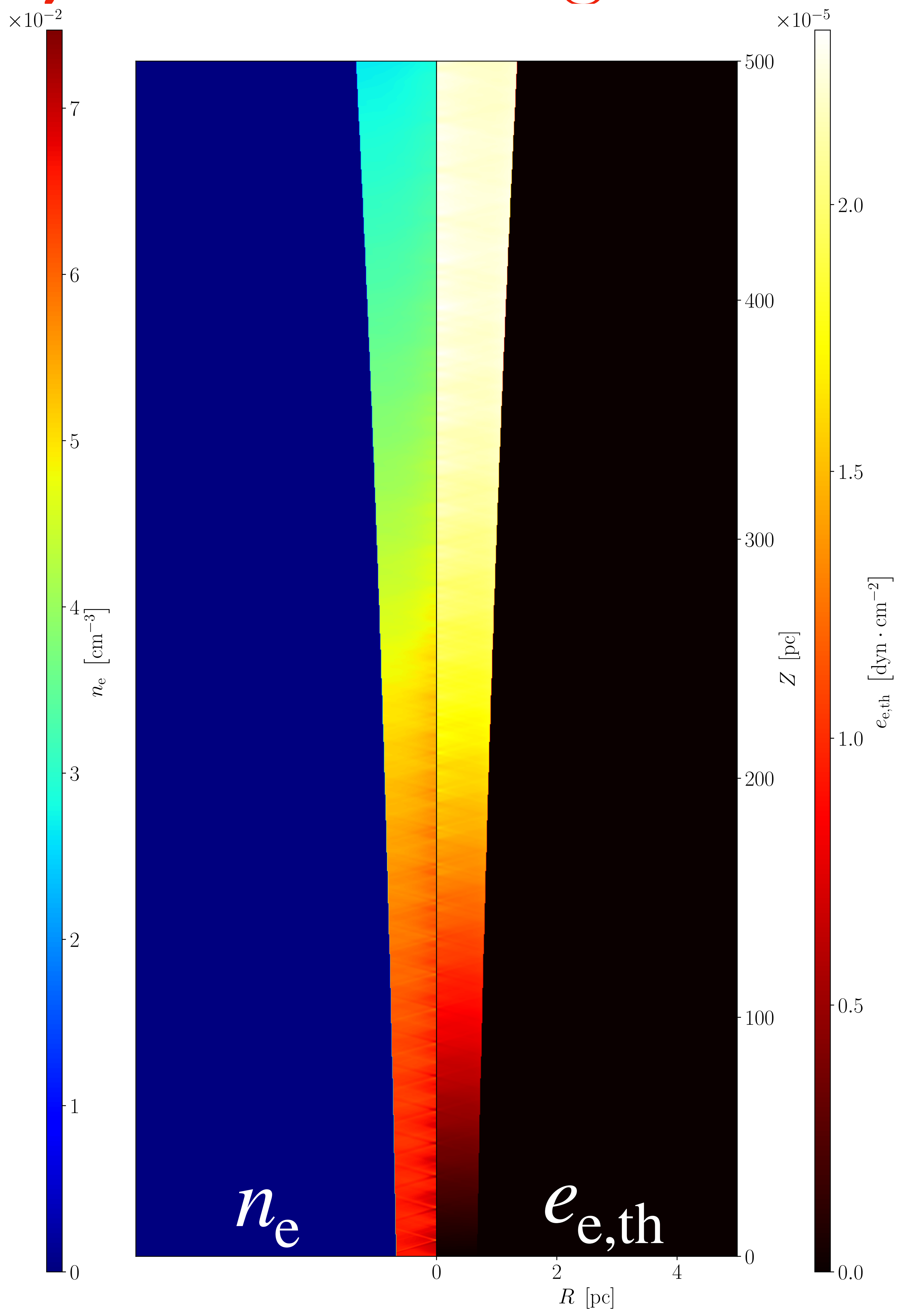

Model J4QC (Anglés-Castillo et al. 2021).

A promising scenario: energy dissipation by mass-loading

Based on the work by Anglés-Castillo, Perucho et al. 2021:

- Simulations of 2000 pc long jets from quasi-1D simulations (Komissarov et al. 2015) with $L_{\rm k,jet} = 10^{43}$ erg $\cdot$ s^{-1}.
- Pair plasma jets with mean stellar mass-losses ranging from 2×10^{-12} to 10^{-9} $M_\odot \cdot \mathrm{yr}^{-1}$, for different gas of stellar distribution $(r_c, r_{c,s})$ that can range from 0.5 to 1.5 kpc.
- Increase of the thermal energy at long distance from the jet base (Bowman et al. 1996), and dilution of e^-, e^+ from mass-loading of protons.
- Large enough mass loading causes jet expansion and deceleration: **promising scenario for radio-galaxy morphologies.**

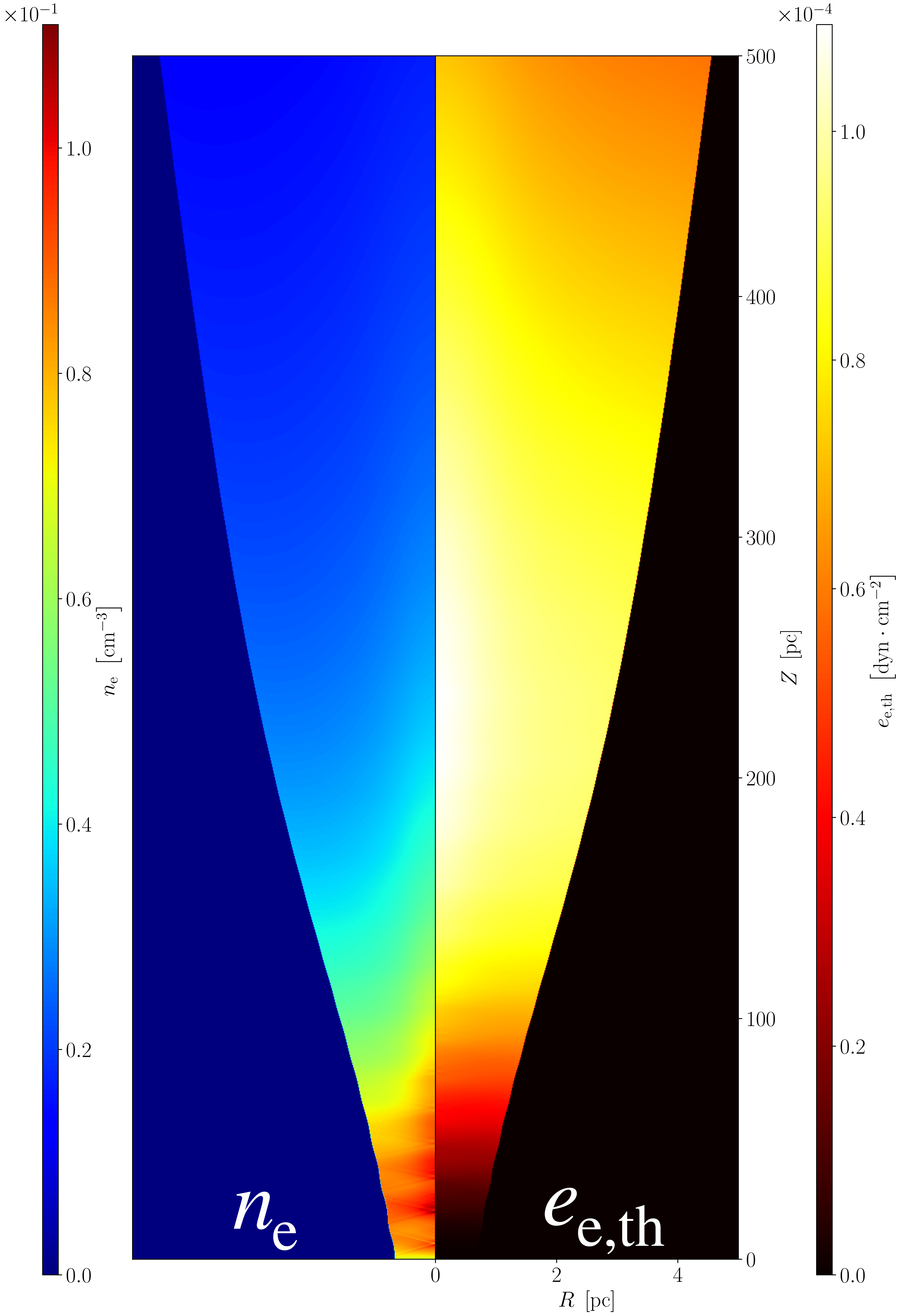

Model J4RA (Anglés-Castillo et al. 2021).

The radio-optical emission offsets

- Gaia Data Release 2 confirmed VLBI-*Gaia* centroid align with the jet direction and 73% of the objects show a positive offset (Plavin et al. 2019).
- VLBI-*Gaia* positive offsets suggest presence of bright and extended optical jets, with projected length of 20 – 50 pc.

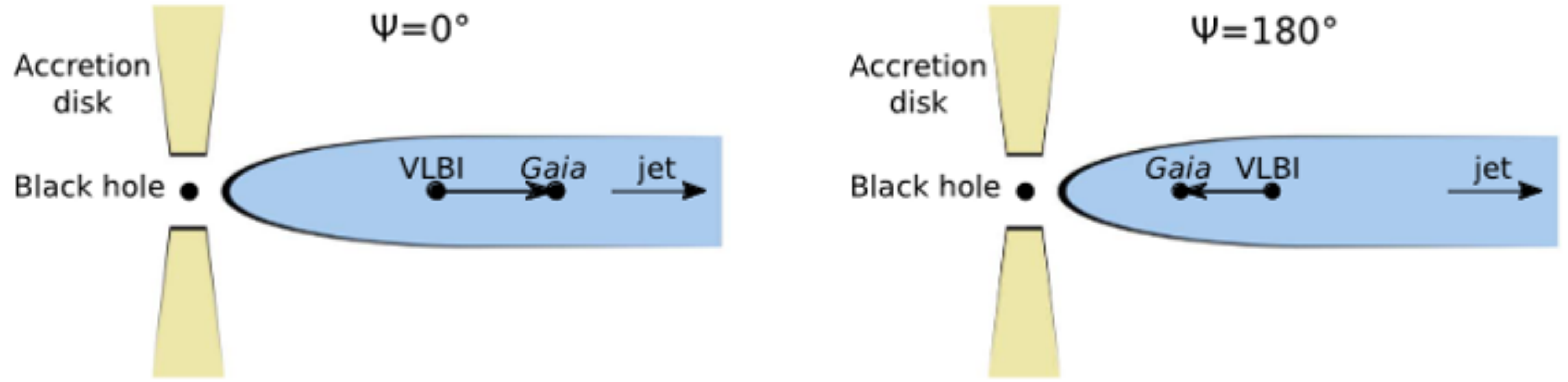

Figure 1. Cartoon explaining two opposite VLBI-to-*Gaia* offset directions with respect to the parsec-scale jet: downstream $\Psi = 0°$ and upstream $\Psi = 180°$.

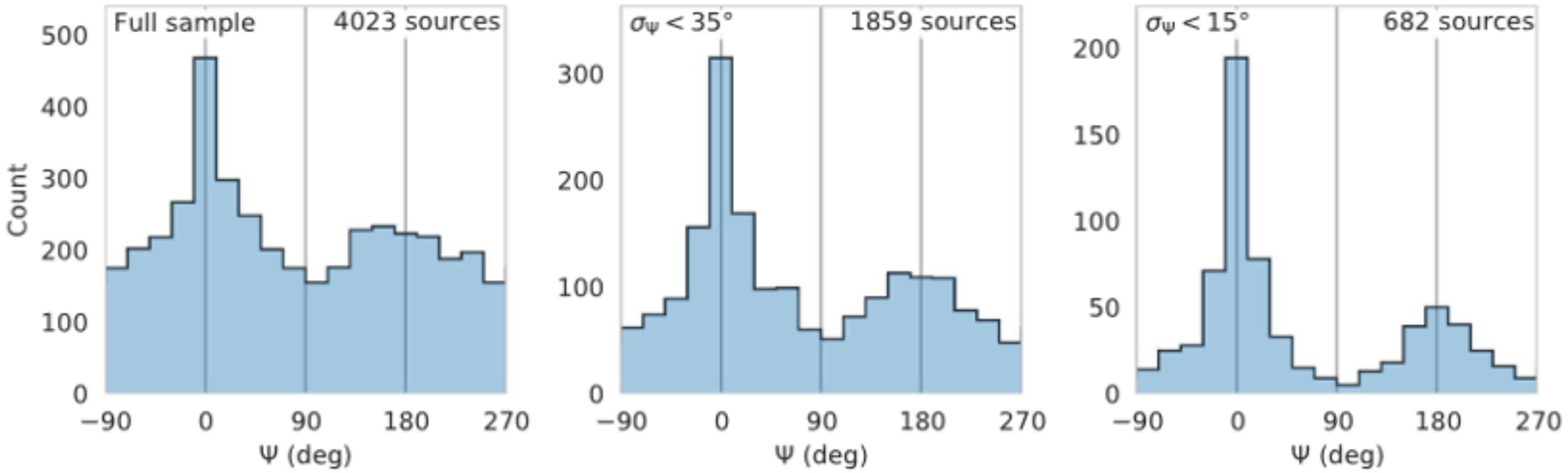

Taken from Plavin et al. 2019.

The radio-optical emission offsets

- Gaia Data Release 2 confirmed VLBI-*Gaia* centroid align with the jet direction and 73% of the objects show a positive offset (Plavin et al. 2019).
- VLBI-*Gaia* positive offsets suggest presence of bright and extended optical jets, with projected length of 20 – 50 pc.

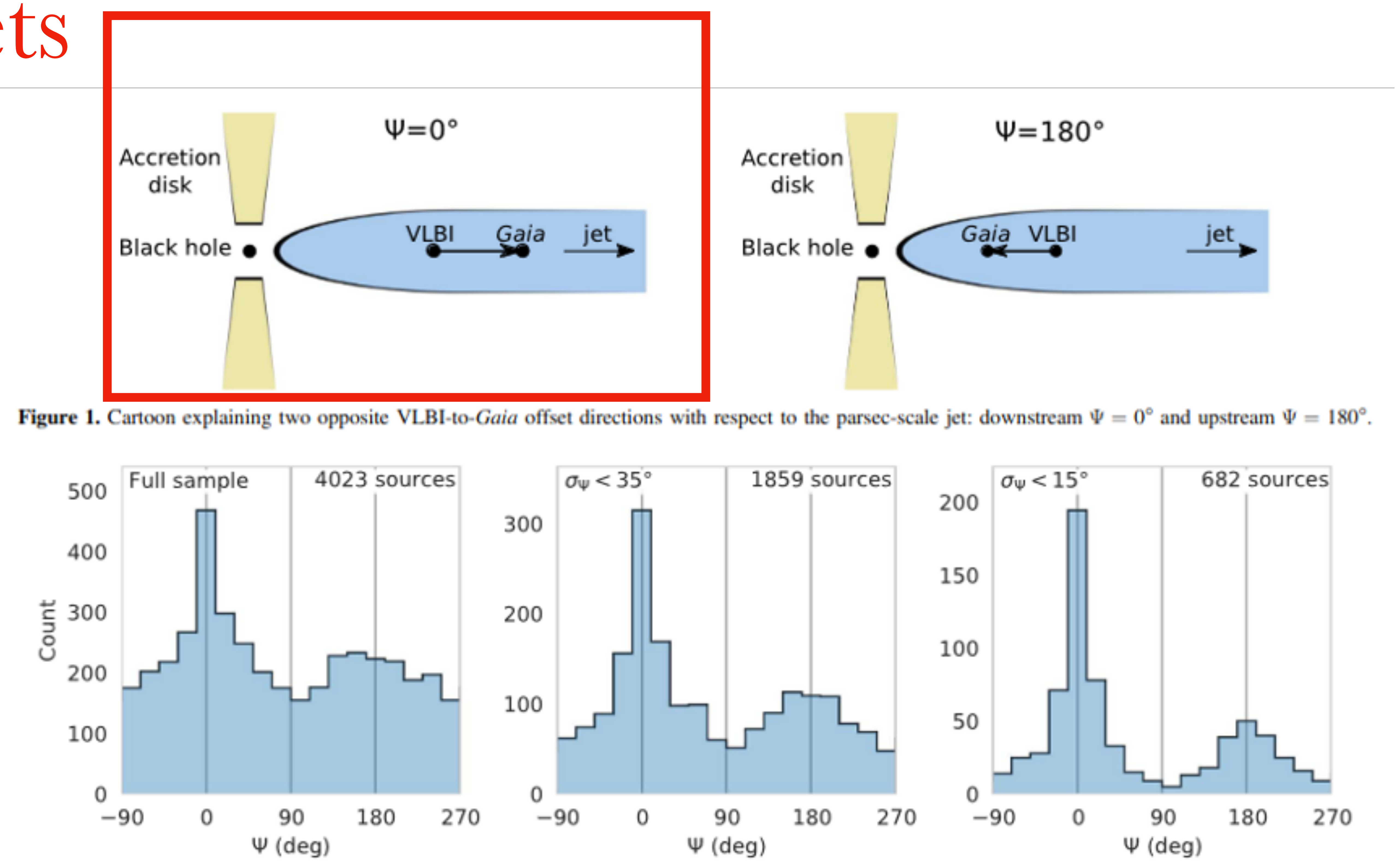

Taken from Plavin et al. 2019.

The radio-optical emission offsets

- Gaia Data Release 2 confirmed VLBI-*Gaia* centroid align with the jet direction and 73% of the objects show a positive offset (Plavin et al. 2019).
- VLBI-*Gaia* positive offsets suggest presence of bright and extended optical jets, with projected length of 20 – 50 pc.

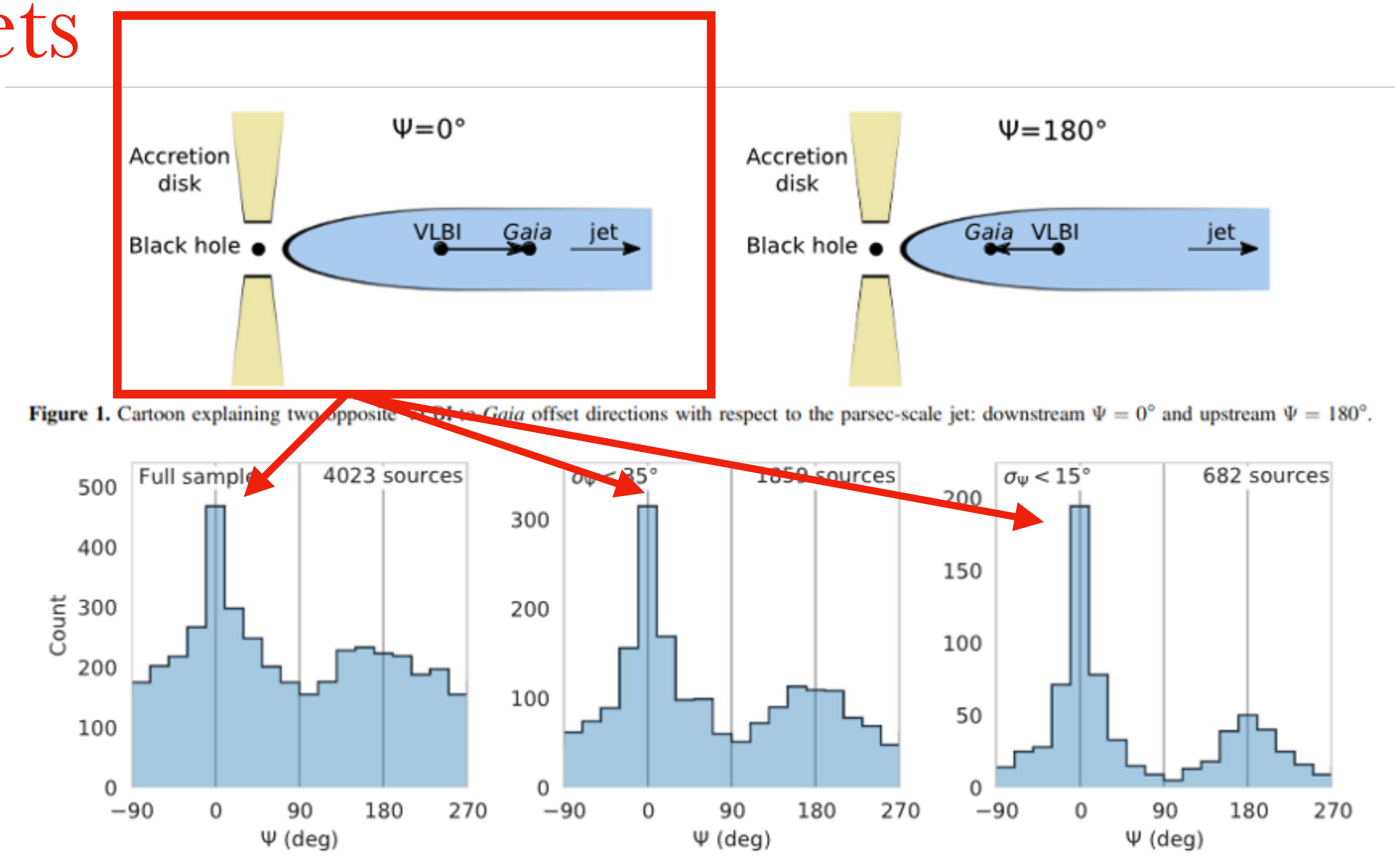

Taken from Plavin et al. 2019.

The radio-optical emission offsets

- Gaia Data Release 2 confirmed VLBI-*Gaia* centroid align with the jet direction and 73% of the objects show a positive offset (Plavin et al. 2019).
- VLBI-*Gaia* positive offsets suggest presence of bright and extended optical jets, with projected length of 20 – 50 pc.

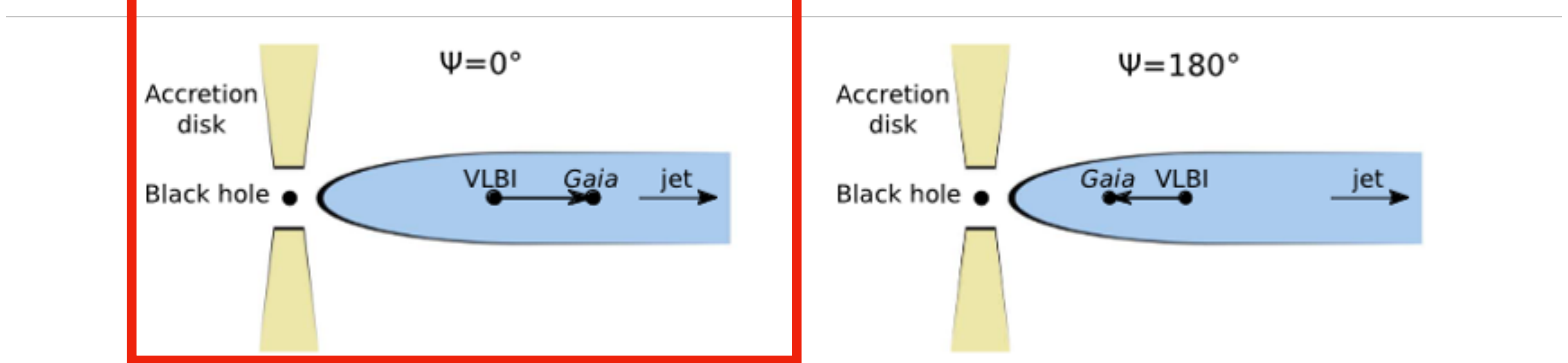

Figure 1. Cartoon explaining two opposite VLBI-to-*Gaia* offset directions with respect to the parsec-scale jet: downstream $\Psi = 0°$ and upstream $\Psi = 180°$.

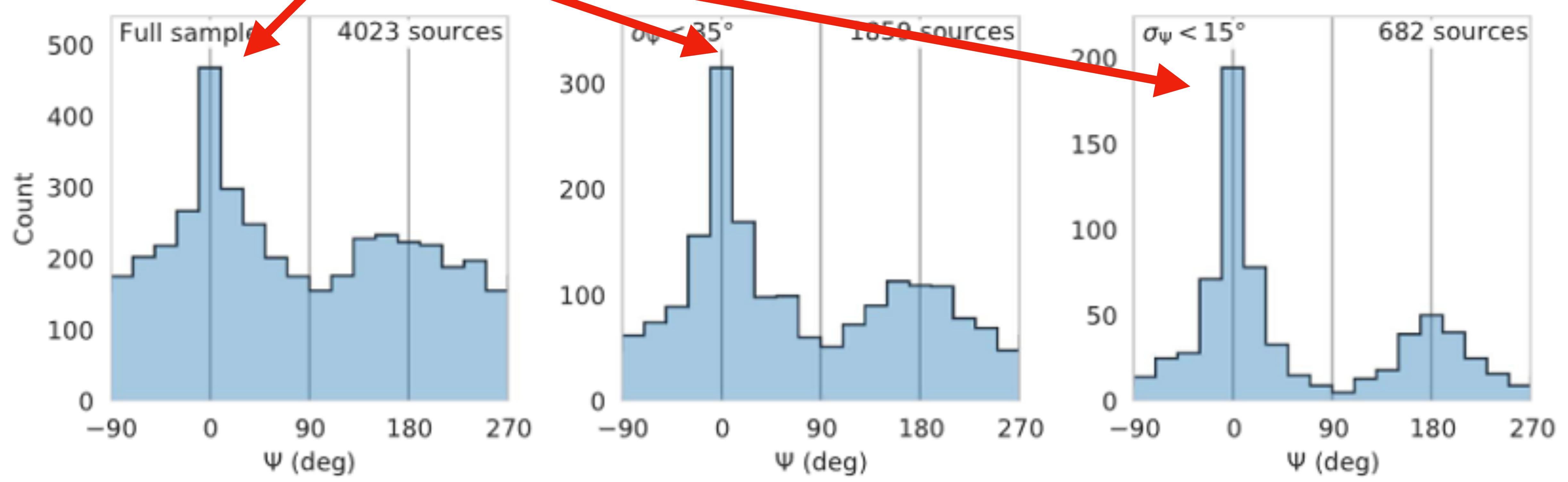

Taken from Plavin et al. 2019.

Positive radio-optical shifts suggest presence of dissipation processes happening down the jet.

Is energy dissipation through mass-loading explain the multiwalength jet morphology?

Radiative transfer: the RIPTIDE code

The RIPTIDE (Fichet DC et al. 2021, 2022) code :

- Convert simulation file (2D) in 3D simulation box.
- In each cell :
  - n_e ($n_e = K\gamma_e^{-p}$) + $e_{e,th}$ = $\gamma_{e,min}$ and $\gamma_{e,max}$ from Gomez et al. 1995.
- Prescription on $\gamma_{e,min}$ based on previous work with similar procedures (Mimica et al. 2012, Fromm et al. 2016, Fichet de Clairfontaine et al. 2021).
- Synchrotron parameters from Katarzynski et al. 2001,
  - Approximations to gain computation time.

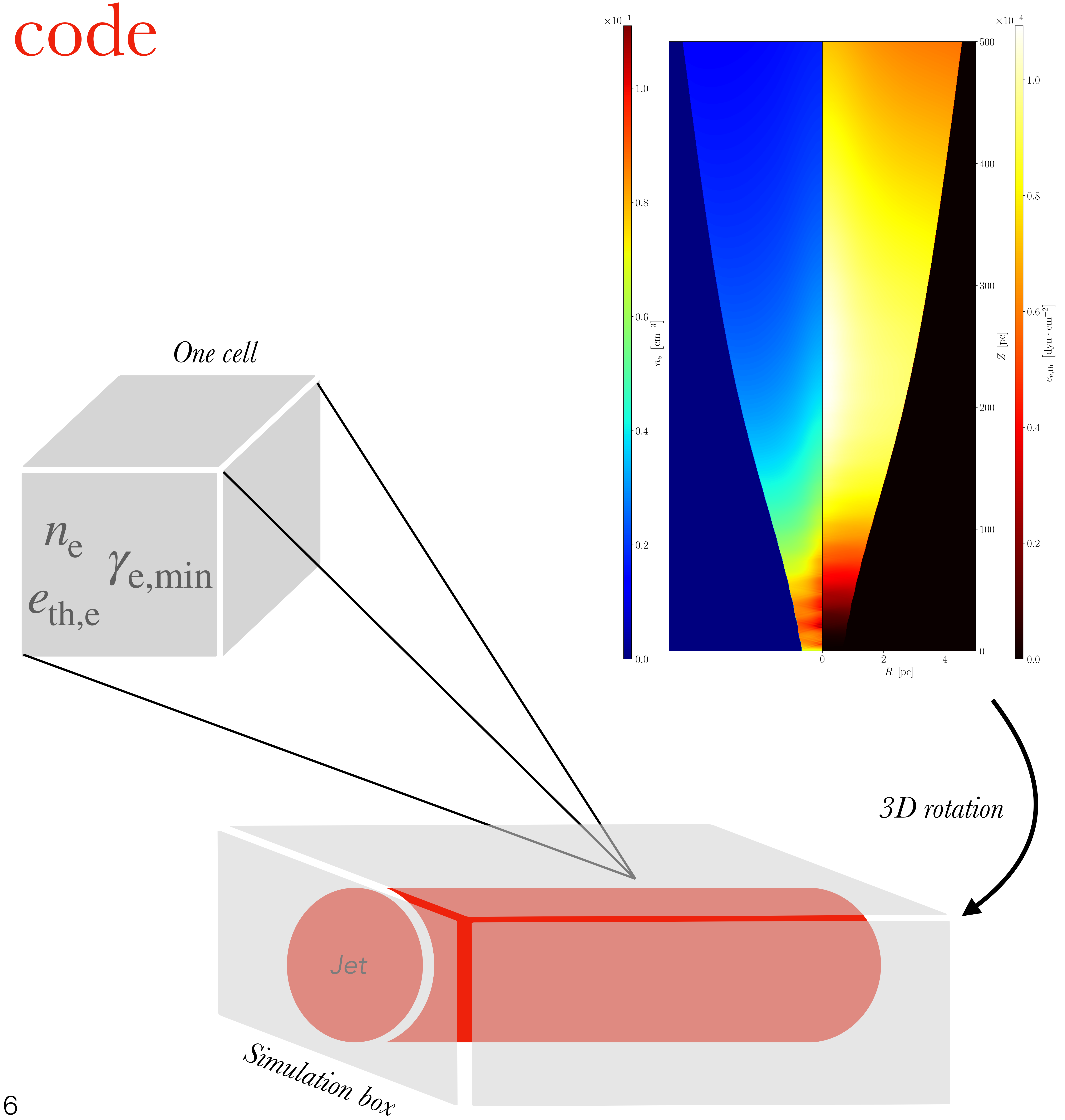

Radiative transfer: the RIPTIDE code

The RIPTIDE (Fichet DC et al. 2021, 2022) code :

- Convert simulation file (2D) in 3D simulation box.
- In each cell :
  - n_e ($n_e = K\gamma_e^{-p}$) + $e_{e,th}$ = $\gamma_{e,min}$ and $\gamma_{e,max}$ from Gomez et al. 1995.
- Prescription on $\gamma_{e,min}$ based on previous work with similar procedures (Mimica et al. 2012, Fromm et al. 2016, Fichet de Clairfontaine et al. 2021).
- Synchrotron parameters from Katarzynski et al. 2001,
  - Approximations to gain computation time.

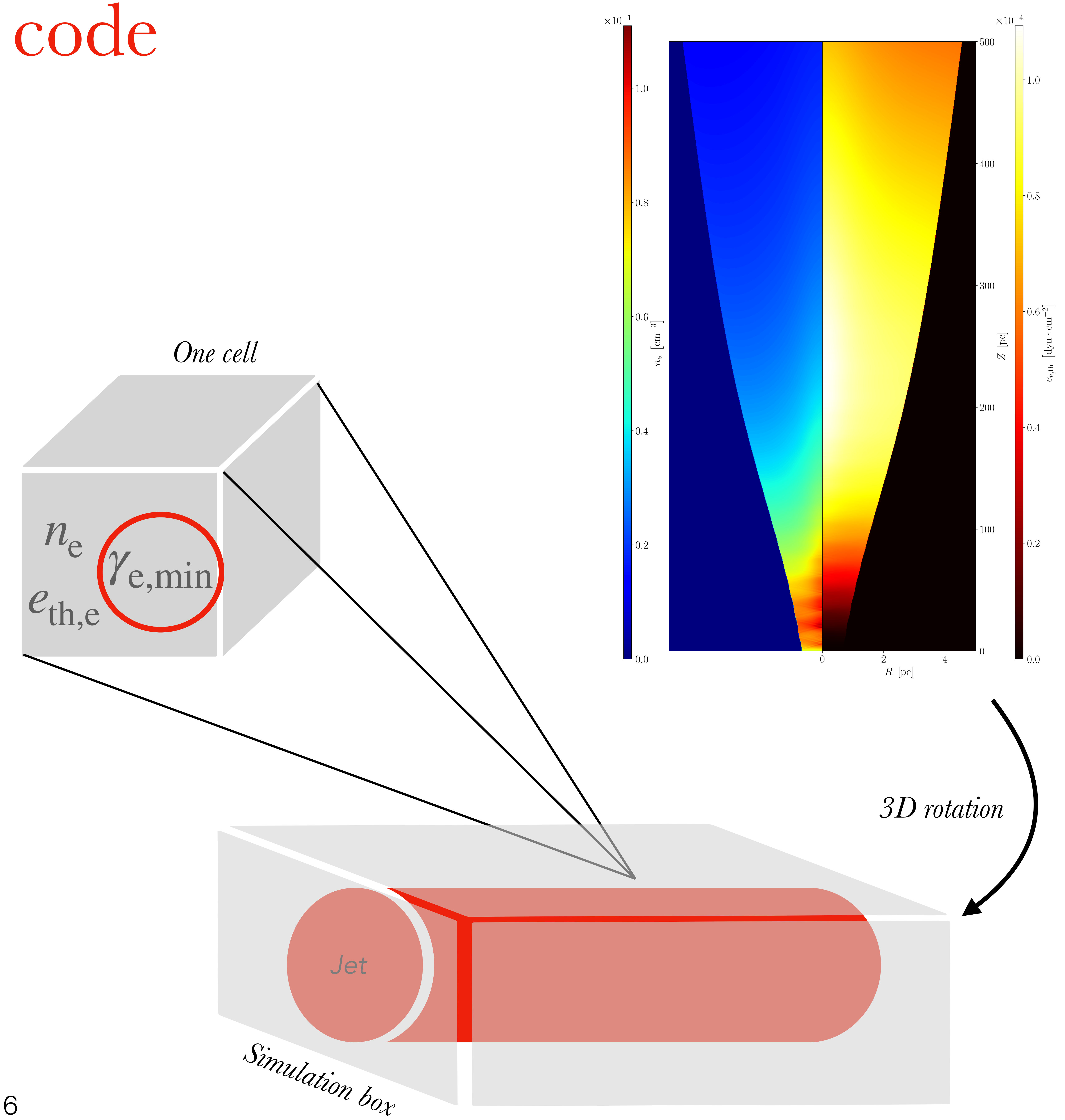

Radiative transfer: the RIPTIDE code

The RIPTIDE (Fichet DC et al. 2021, 2022) code :

- Convert simulation file (2D) in 3D simulation box.
- In each cell :
  - n_e ($n_e = K\gamma_e^{-p}$) + $e_{e,th}$ = $\gamma_{e,min}$ and $\gamma_{e,max}$ from Gomez et al. 1995.
- Prescription on $\gamma_{e,min}$ based on previous work with similar procedures (Mimica et al. 2012, Fromm et al. 2016, Fichet de Clairfontaine et al. 2021).
- Synchrotron parameters from Katarzynski et al. 2001,
  - Approximations to gain computation time.

$$\gamma_{e,min} = \frac{1}{m_e c^2} \frac{e_{e,th}}{n_e} \frac{p-2}{p-1} \frac{1 - C_E^{1-p}}{1 - C_E^{2-p}}$$

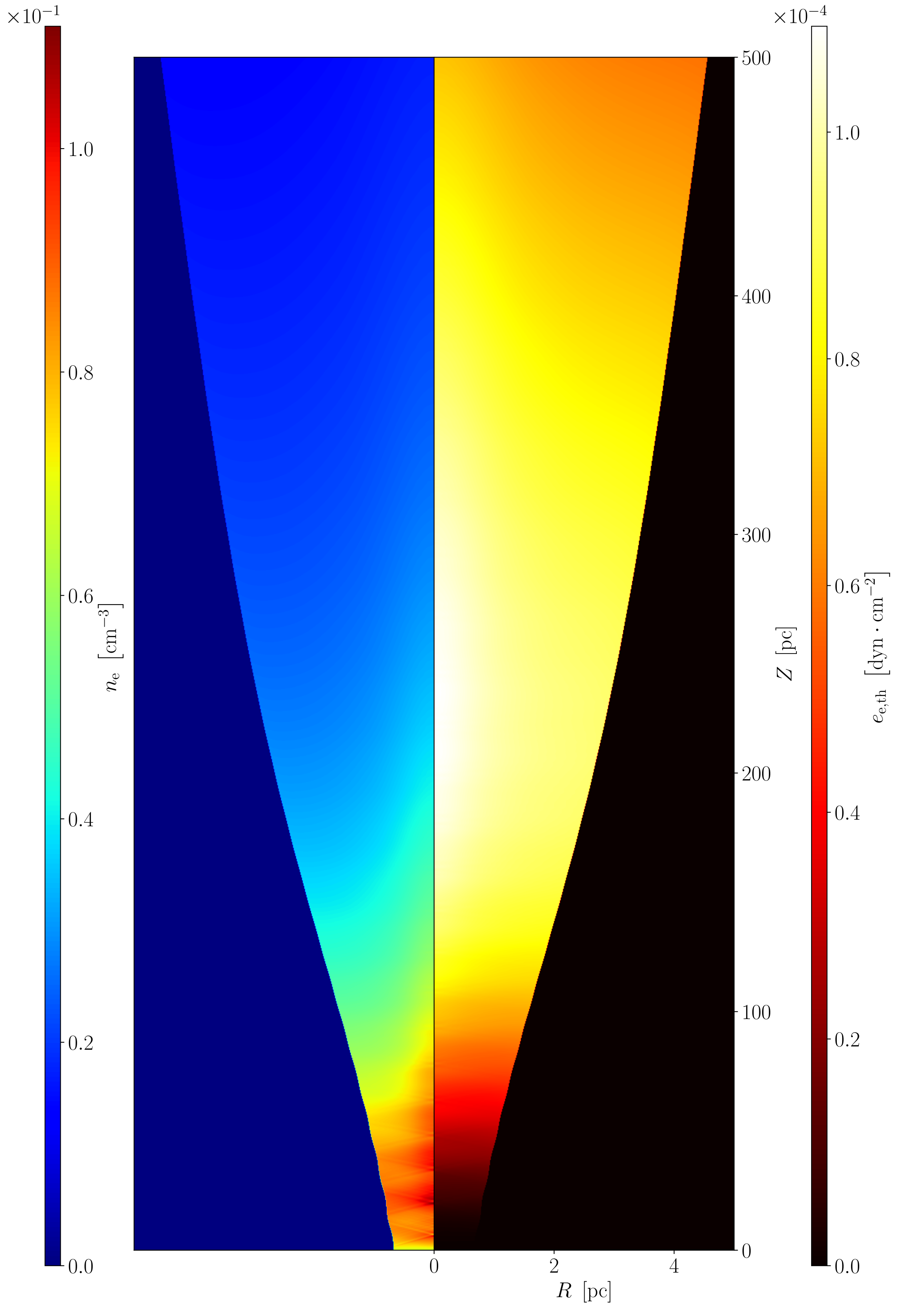

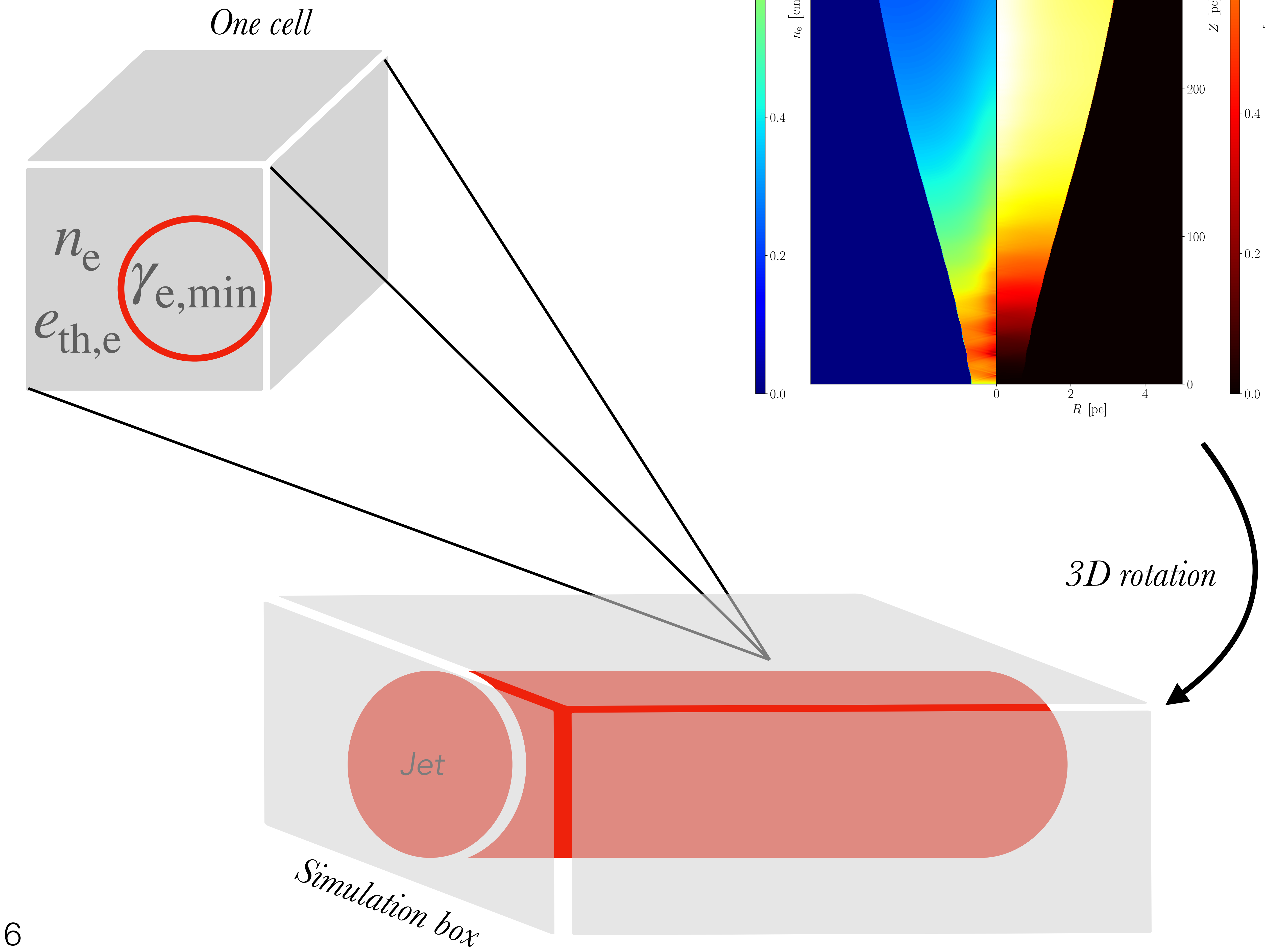

Radiative transfer: the RIPTIDE code

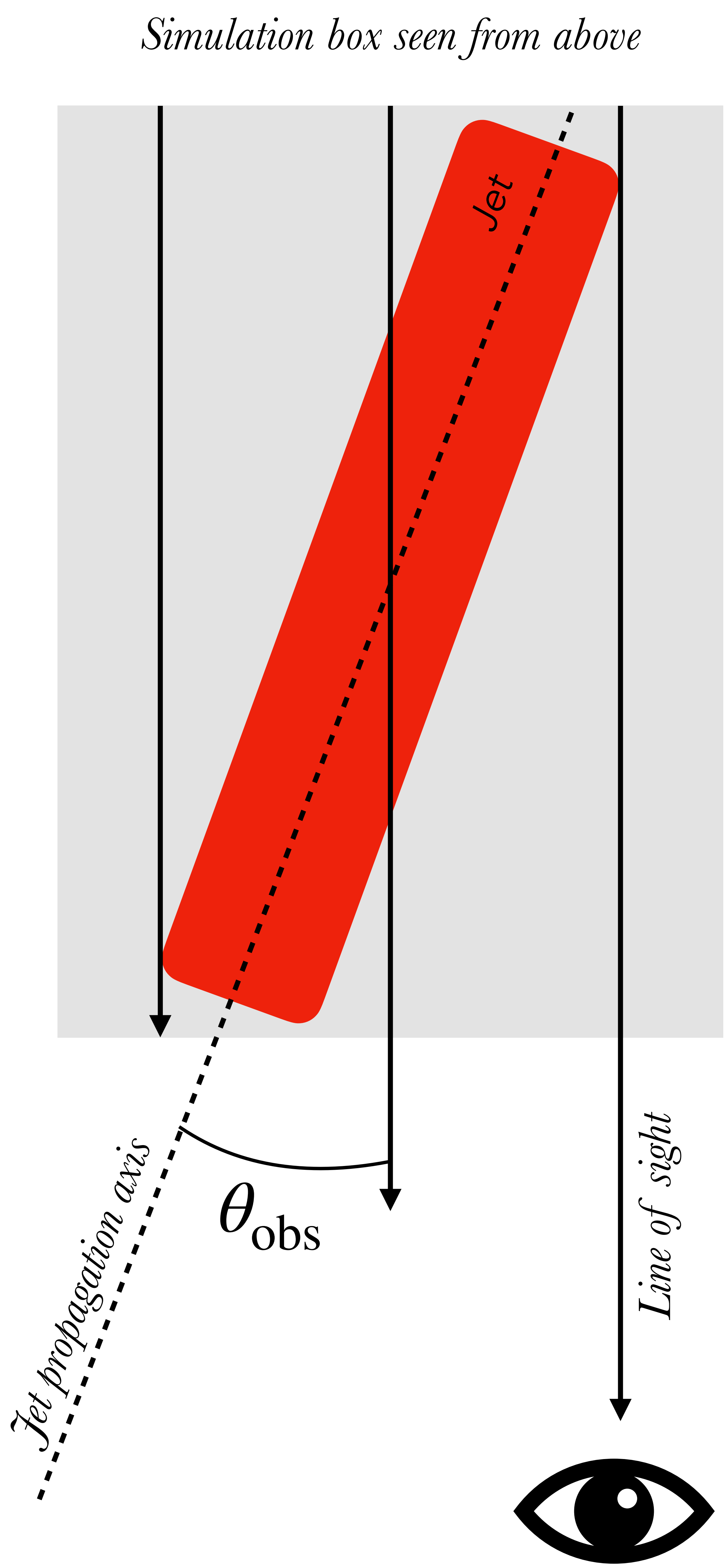

The RIPTIDE (Fichet DC et al. 2021, 2022) code :

- Rotation of the emission maps according to θ_{obs}.
- Doppler boosting according to θ_{obs} and local γ_{j}, allowing us to transform useful quantities in the observer's frame.
- Integration of the emission "face-on" along the line of sight,

$$I_{\nu;\text{i}} = I_{\nu;\text{i}-1} \exp\left(-\tau_{\nu;\text{i}}\right) + S_{\nu;\text{i}} \left(1 - \exp\left(-\tau_{\nu;\text{i}}\right)\right).$$

- Distance between the source and the Earth,

$$F_{\nu} = \frac{S_{\text{pix}}}{D_{\text{L}}^2} (1+z)\, I_{\nu}\,.$$

Radio-optical emission maps

Computation of radio $(3 \times 10^{11}$ Hz$)$ **and optical** $(5 \times 10^{14}$ Hz$)$ **synchrotron maps:**

- Flux selection criteria from the *Gaia* mission $(F_\nu \geq 10^{-4}$ Jy$)$ and in the radio (VLBI - $F_\nu \geq 10^{-3}$ Jy).
- Positive shifts are observed depending on the mass loading profiles and on the stellar distribution $r_{c,s}$
  - Shift distance spanned between 0 – 100 pc (de-projected).
- Some simulations show null or negative shifts, consistent with pure adiabatic cooling of electrons.

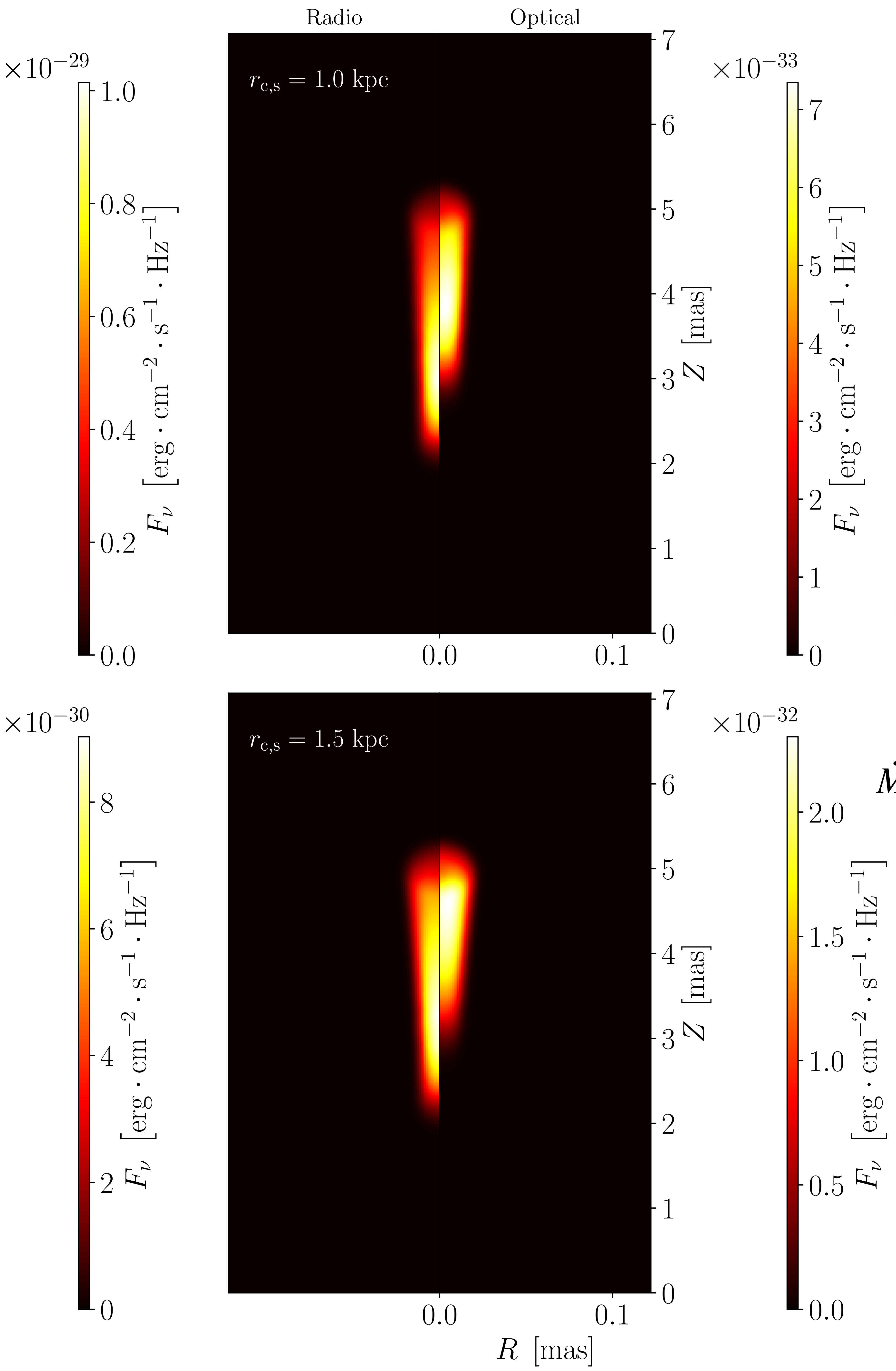

$\theta_{obs} = 5°$

$z = 1.4$

$\dot{M} = 10^{-10}\ M_\odot \cdot$ yr^{-1}

Radio-optical offsets

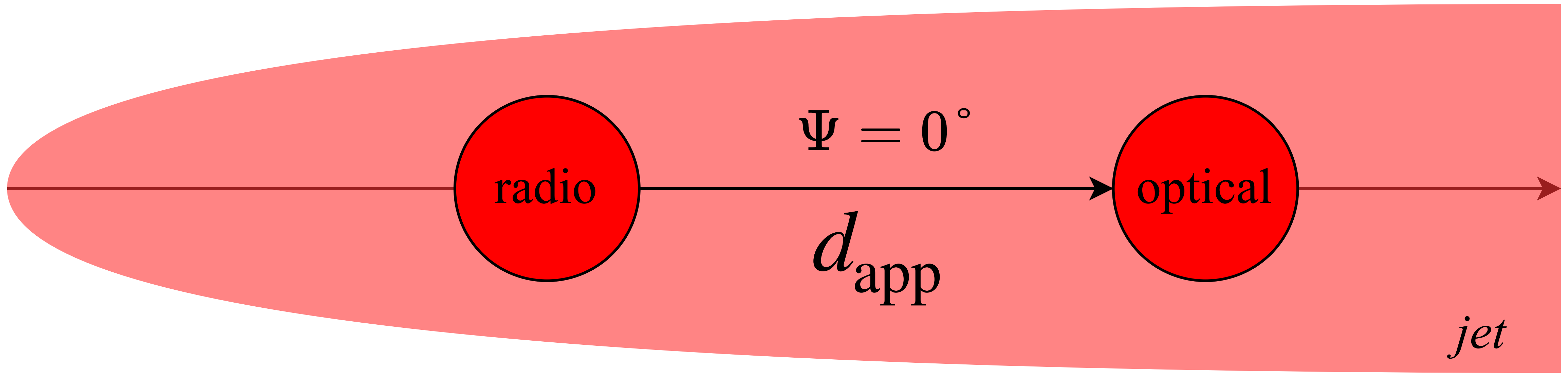

Histogram of shift positions / angles reveals:

- 1000 simulations done with random θ_{obs} and z for various values of $\dot{M}$.
- Only a limited amount of simulations have a detectable optical emission by *Gaia* and a non zero shift.
- Distribution of sources centred on $\Psi \sim 0°$ with a tail that evolves with $\dot{M}$.

Evolution of d_{app} for a fix $\dot{M}$ shows:

- Impact of gas / stellar distribution. For high $\dot{M}$, the offset converge to zero.
- $d_{app} > 0$ mas emerge in an average mass-loss rate between $\dot{M} \sim \left[10^{-11}, 10^{-10}\right]\ M_\odot \cdot yr^{-1}$.

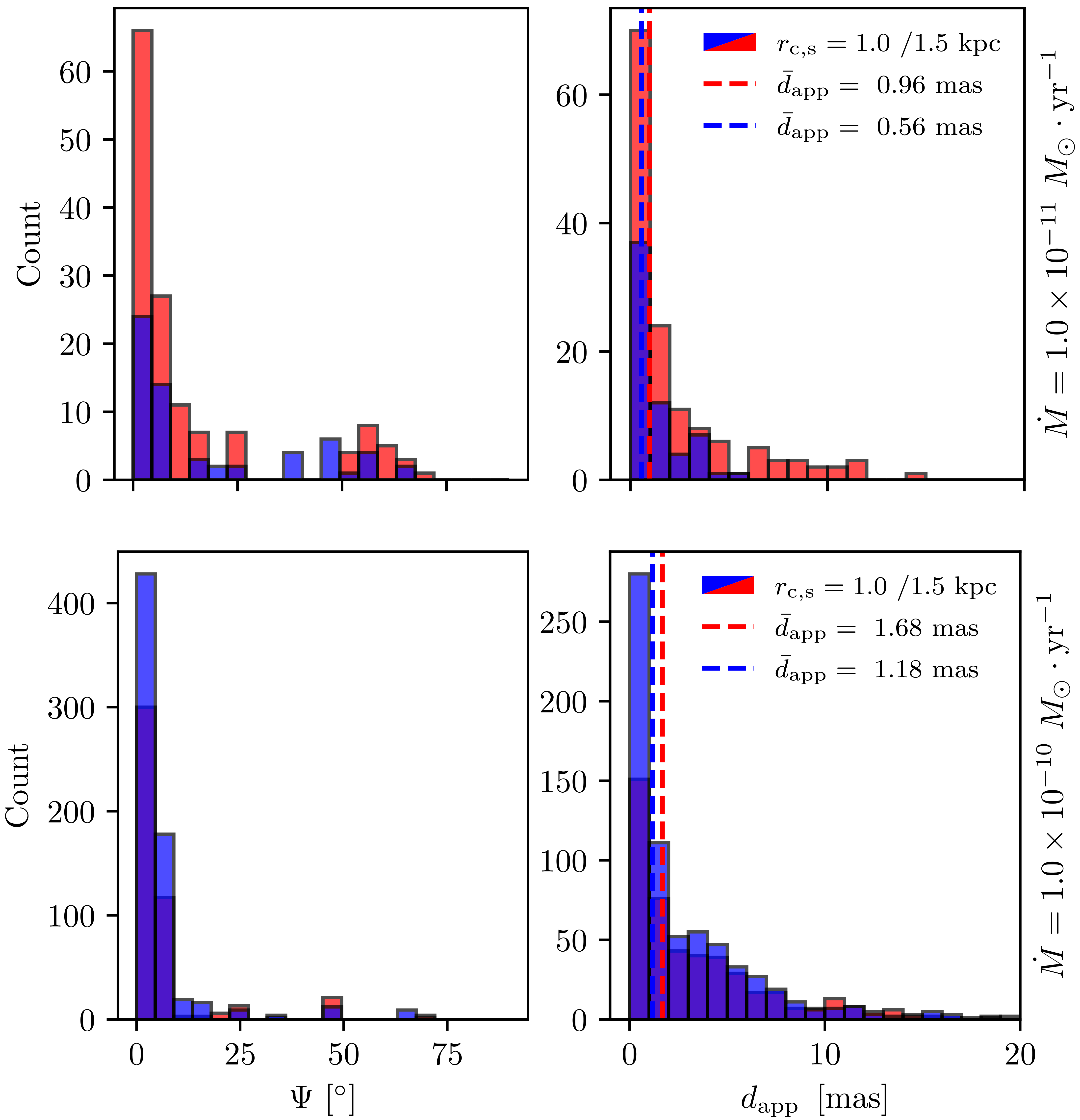

Radio-optical offsets

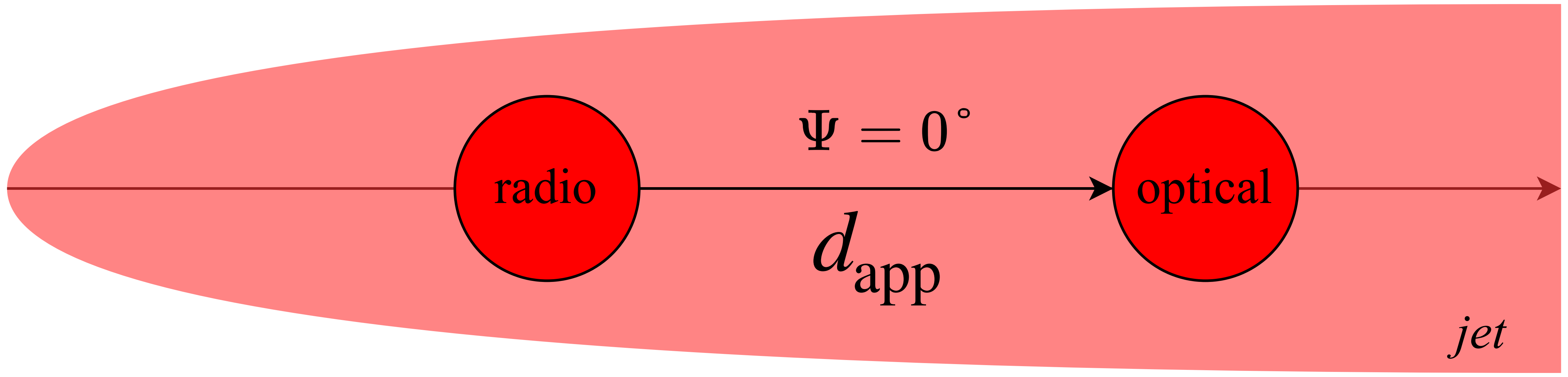

Histogram of shift positions / angles reveals:

- 1000 simulations done with random θ_{obs} and z for various values of $\dot{M}$.
- Only a limited amount of simulations have a detectable optical emission by *Gaia* and a non zero shift.
- Distribution of sources centred on $\Psi \sim 0°$ with a tail that evolves with $\dot{M}$.

Evolution of d_{app} for a fix $\dot{M}$ shows:

- Impact of gas / stellar distribution. For high $\dot{M}$, the offset converge to zero.
- $d_{app} > 0$ mas emerge in an average mass-loss rate between $\dot{M} \sim [10^{-11}, 10^{-10}]\ M_\odot \cdot yr^{-1}$.

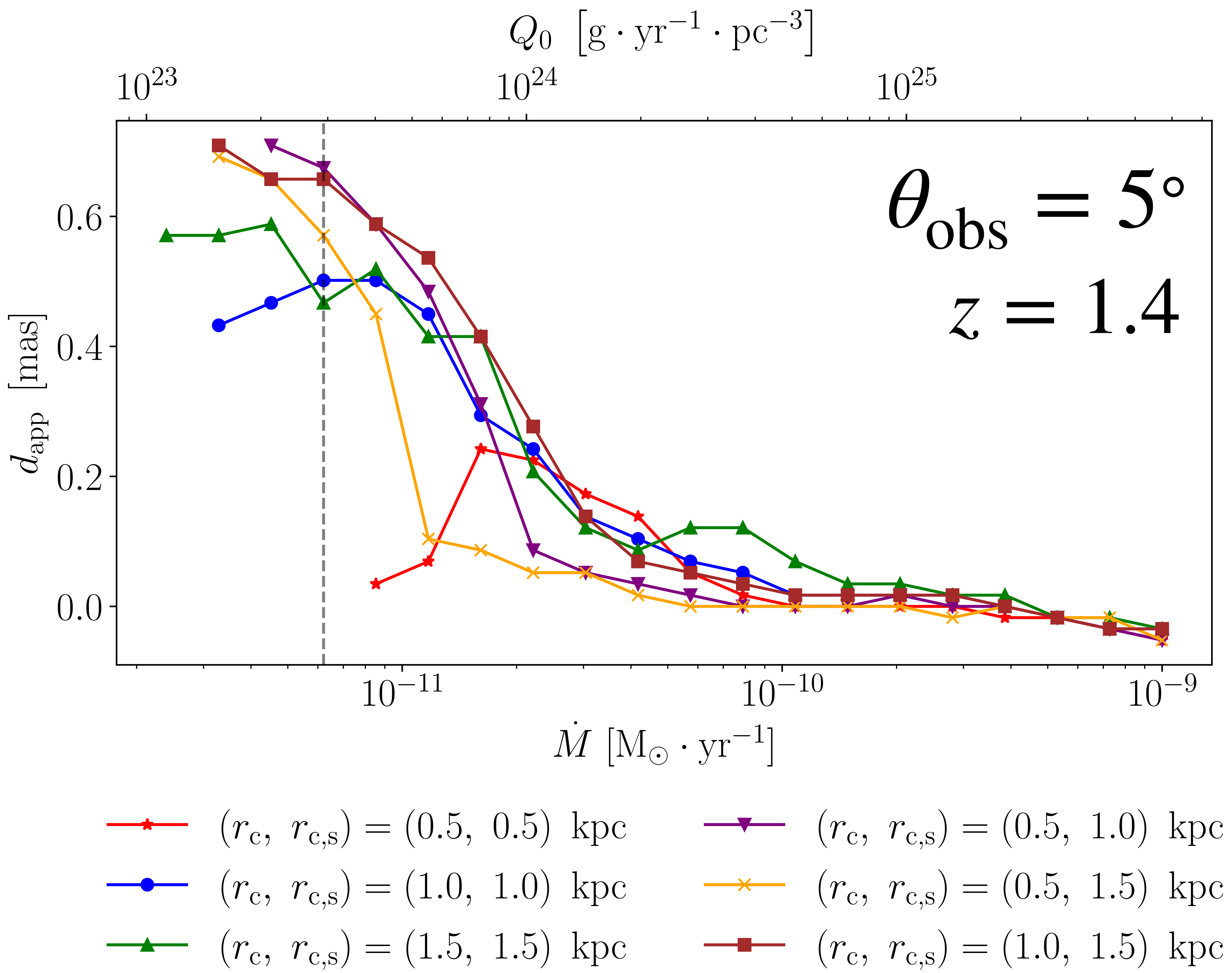

Radio-optical offsets

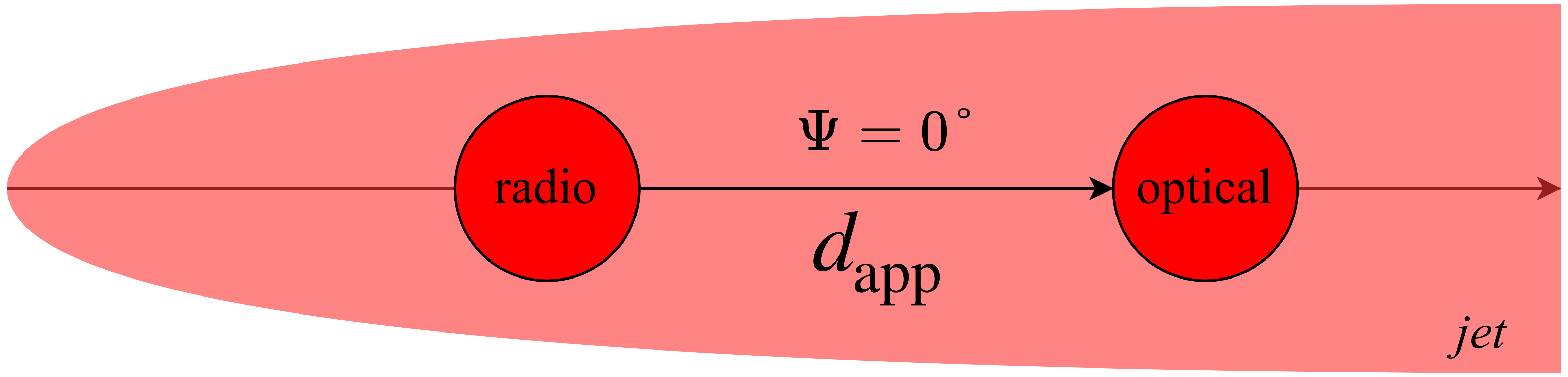

Histogram of shift positions / angles reveals:

- 1000 simulations done with random θ_{obs} and z for various values of $\dot{M}$.
- Only a limited amount of simulations have a detectable optical emission by *Gaia* and a non zero shift.
- Distribution of sources centred on $\Psi \sim 0°$ with a tail that evolves with $\dot{M}$.

Evolution of d_{app} for a fix $\dot{M}$ shows:

- Impact of gas / stellar distribution. For high $\dot{M}$, the offset converge to zero.
- $d_{app} > 0$ mas emerge in an average mass-loss rate between $\dot{M} \sim [10^{-11}, 10^{-10}]\ M_\odot \cdot yr^{-1}$.

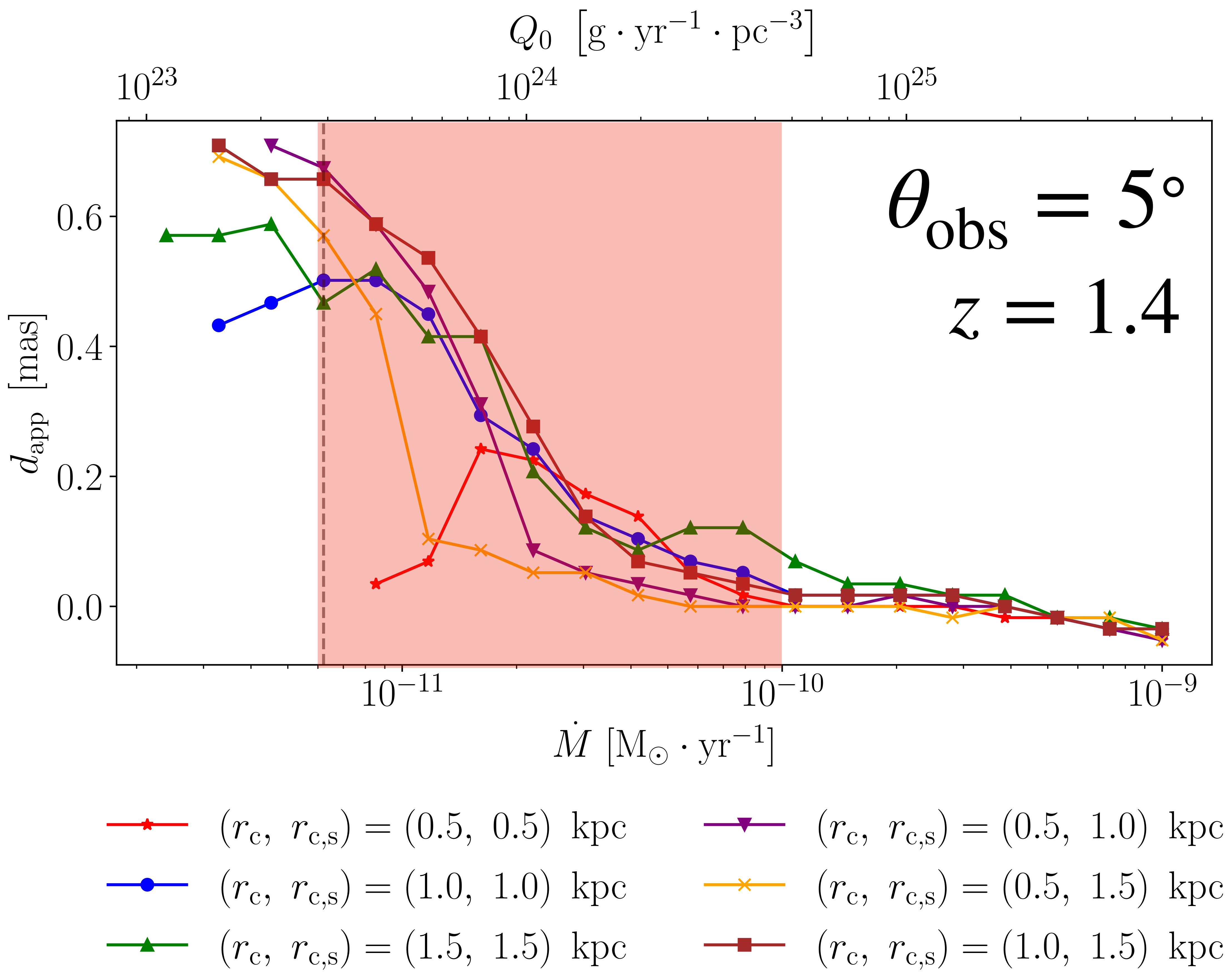

Color magnitude and stellar population

Accretion disks: Bluer optical objects are linked to the presence of an accretion disk, and negative radio-optical offset / redder objects correlate with a positive radio-optical offset (Plavin et al. 2019).

Color magnitude: Larger positive Δm suggests a redder jet, which corresponds to low $\dot{M}$ ⇒ corresponds to higher radio-optical offsets.

Stellar population: The final $\dot{M}$ range corresponds to K/M-type stars which are commonly observed in elliptical galaxies (Ó Fionnagáin et al. 2020).

This population might affect the radio-optical offset and color magnitude, potentially making jets appear redder and with larger offset.

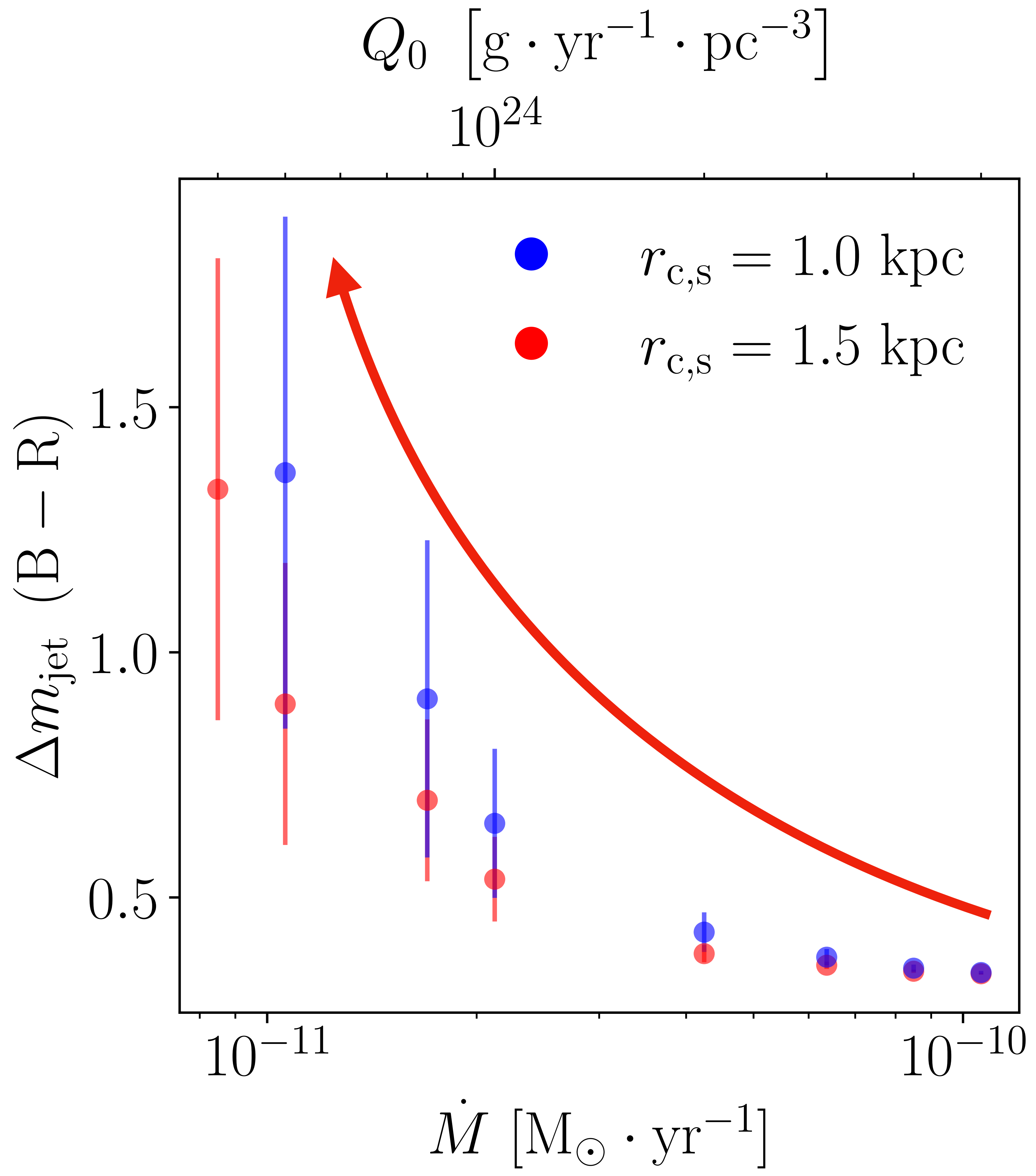

+ potential contribution from a stellar population.

The mass-loading scenario: implications

Observational biases: Doopler boosting plays a major role in regards of the flux selection criteria.

Source type: quasars tends to show near-to-zero offset, observed at low θ_{obs} and higher z, while radio-galaxies and Seyfert at higher θ_{obs} and lower z.

Jet power: Based on optical observations, the offset appears as a unique tool to constraint the jet power.

Gamma-ray emission: Jet-star interactions are often listed to explain gamma-ray emission in jetted AGN (Torres et al. 2019) and in the production of very-energetic cosmic rays (Wykes et al. 2014).

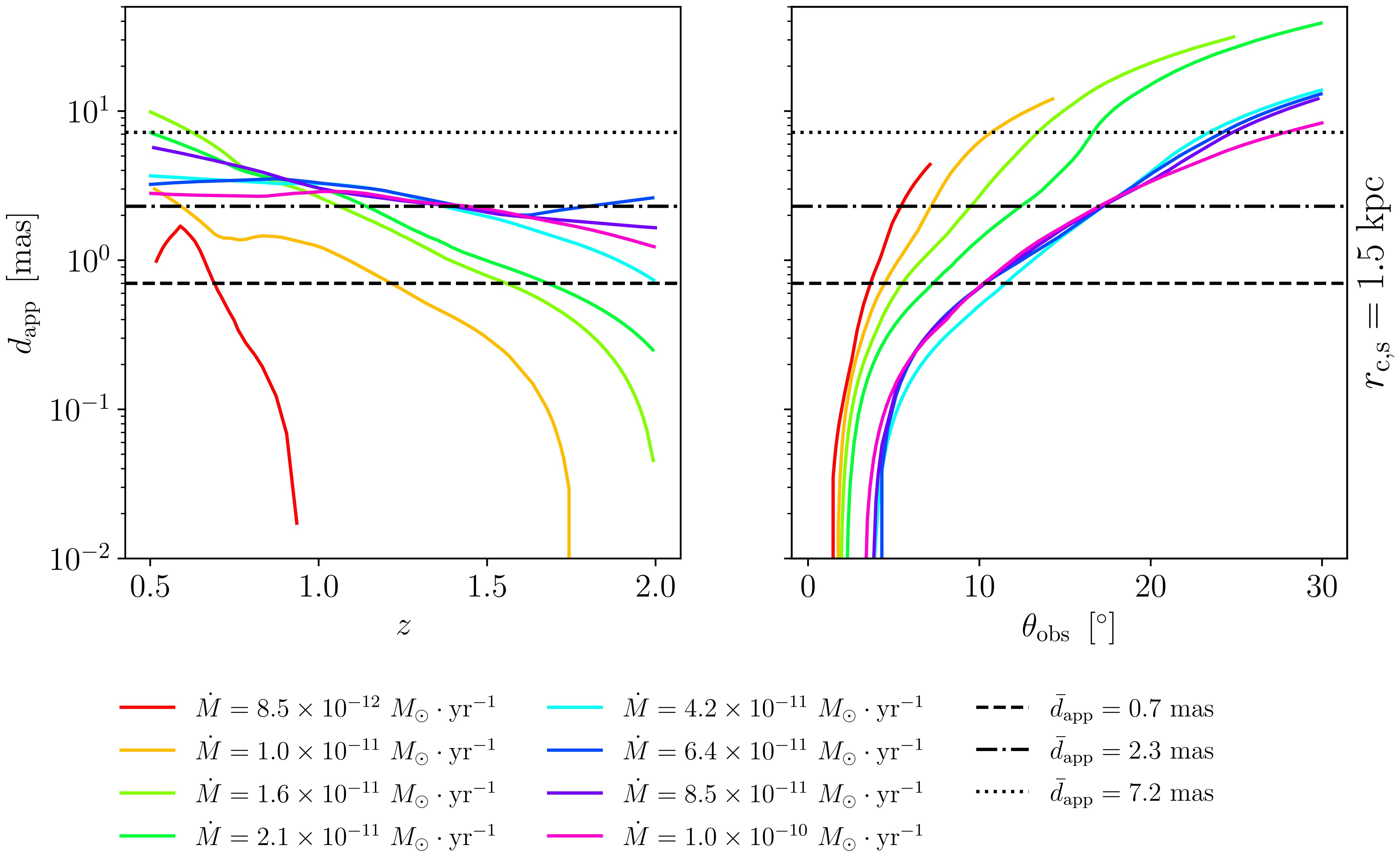

The mass-loading scenario: implications

Observational biases: Doopler boosting plays a major role in regards of the flux selection criteria.

Source type: quasars tends to show near-to-zero offset, observed at low θ_{obs} and higher z, while radio-galaxies and Seyfert at higher θ_{obs} and lower z.

Jet power: Based on optical observations, the offset appears as a unique tool to constraint the jet power.

Gamma-ray emission: Jet-star interactions are often listed to explain gamma-ray emission in jetted AGN (Torres et al. 2019) and in the production of very-energetic cosmic rays (Wykes et al. 2014).

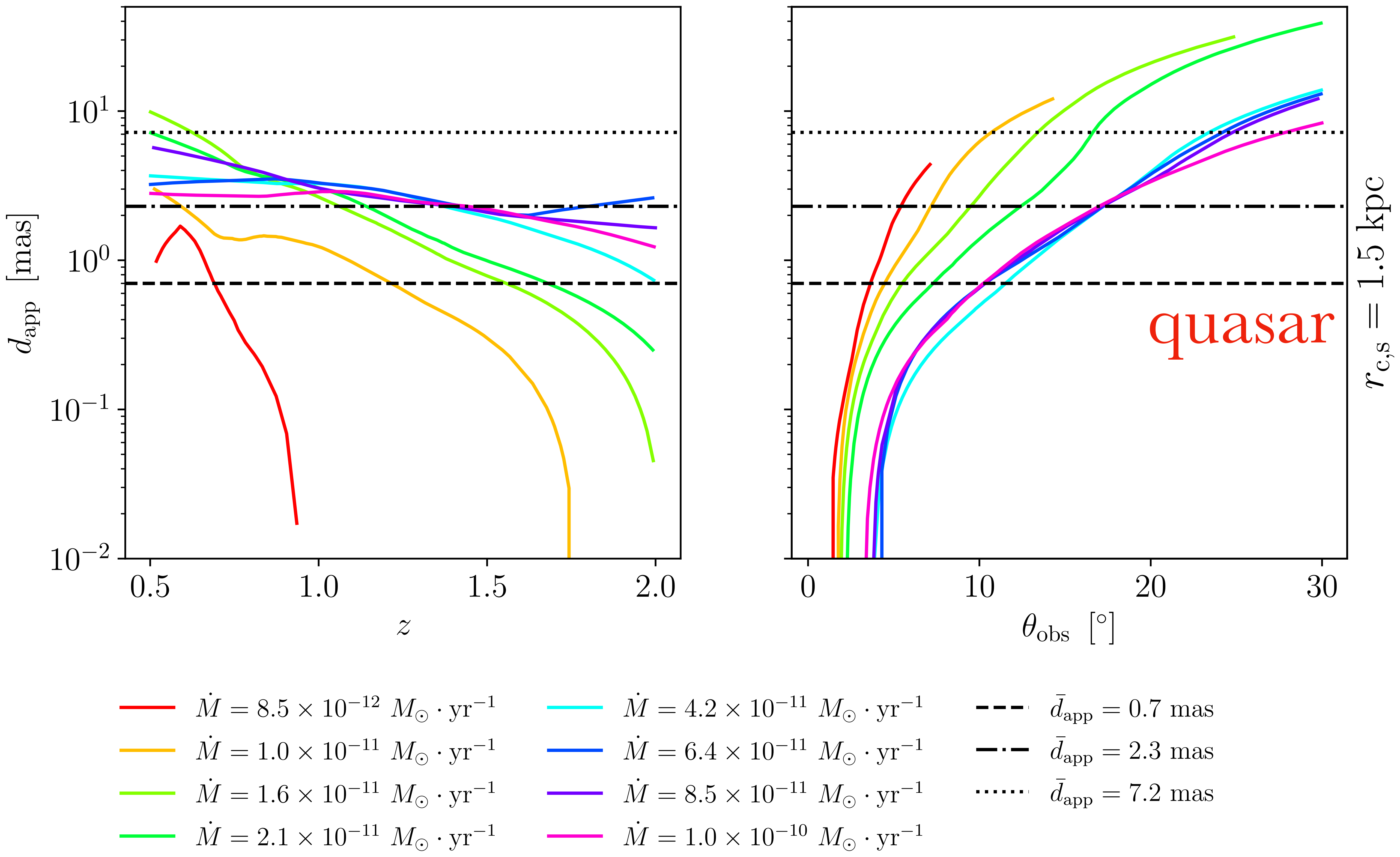

The mass-loading scenario: implications

Observational biases: Doopler boosting plays a major role in regards of the flux selection criteria.

Source type: quasars tends to show near-to-zero offset, observed at low θ_{obs} and higher z, while radio-galaxies and Seyfert at higher θ_{obs} and lower z.

Jet power: Based on optical observations, the offset appears as a unique tool to constraint the jet power.

Gamma-ray emission: Jet-star interactions are often listed to explain gamma-ray emission in jetted AGN (Torres et al. 2019) and in the production of very-energetic cosmic rays (Wykes et al. 2014).

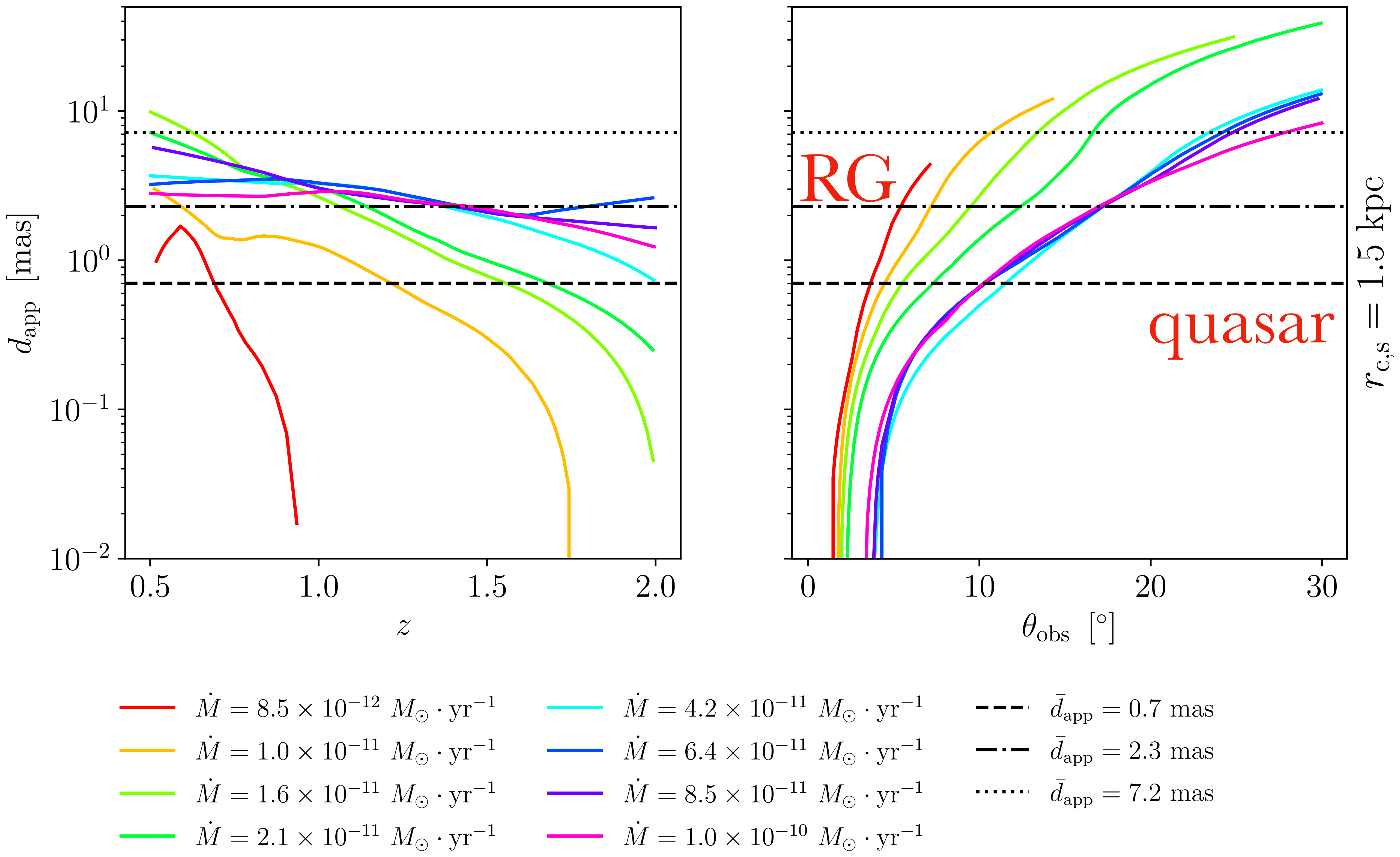

The mass-loading scenario: implications

Observational biases: Doopler boosting plays a major role in regards of the flux selection criteria.

Source type: quasars tends to show near-to-zero offset, observed at low θ_{obs} and higher z, while radio-galaxies and Seyfert at higher θ_{obs} and lower z.

Jet power: Based on optical observations, the offset appears as a unique tool to constraint the jet power.

Gamma-ray emission: Jet-star interactions are often listed to explain gamma-ray emission in jetted AGN (Torres et al. 2019) and in the production of very-energetic cosmic rays (Wykes et al. 2014).

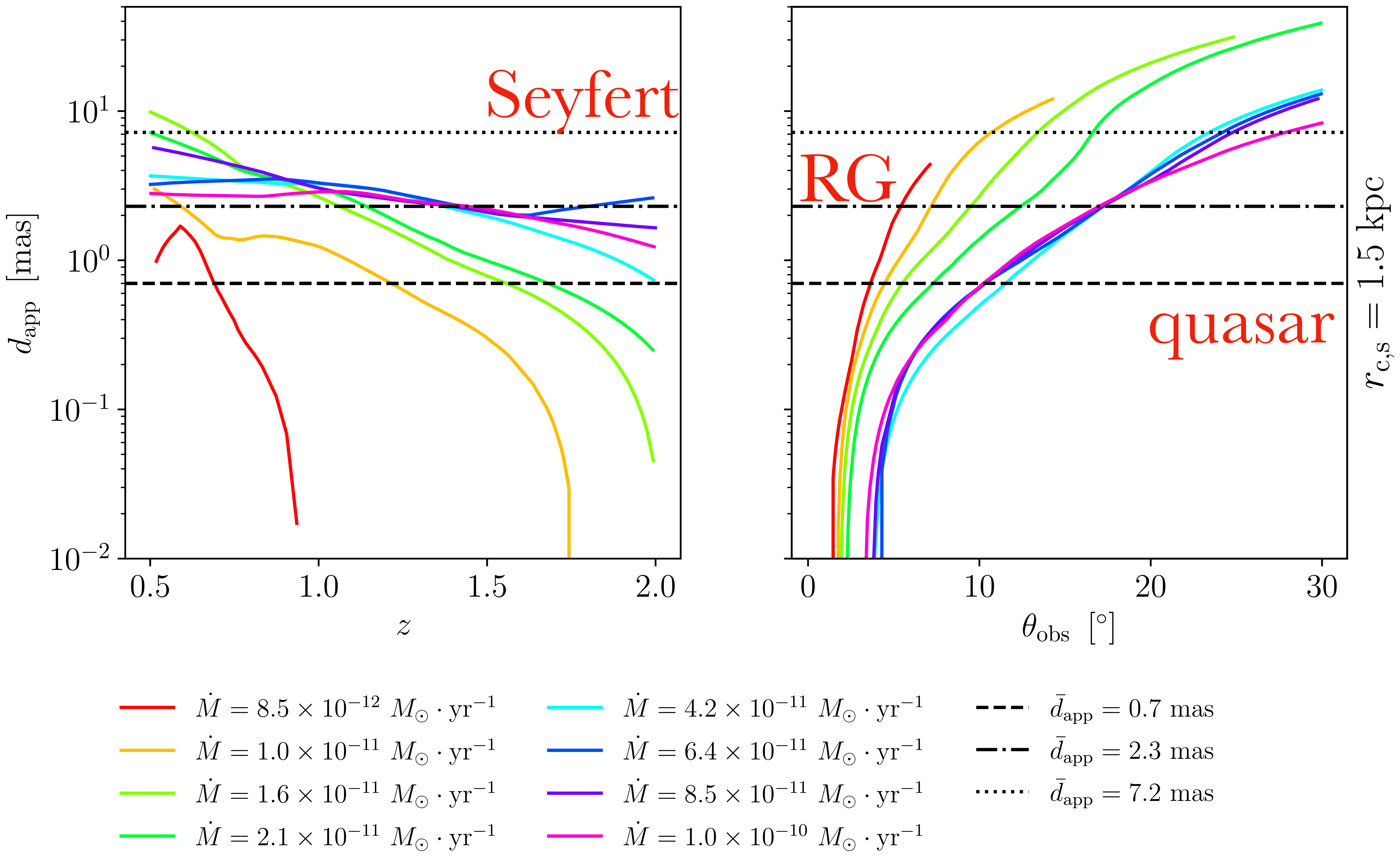

The mass-loading scenario: implications

Poster of Bruno Longo
Parsec-scale simulations of jet-star interaction : dynamical and radiative effects

Observational biases: Doopler boosting plays a major role in regards of the flux selection criteria.

Source type: quasars tends to show near-to-zero offset, observed at low θ_{obs} and higher z, while radio-galaxies and Seyfert at higher θ_{obs} and lower z.

Jet power: Based on optical observations, the offset appears as a unique tool to constraint the jet power.

Gamma-ray emission: Jet-star interactions are often listed to explain gamma-ray emission in jetted AGN (Torres et al. 2019) and in the production of very-energetic cosmic rays (Wykes et al. 2014).

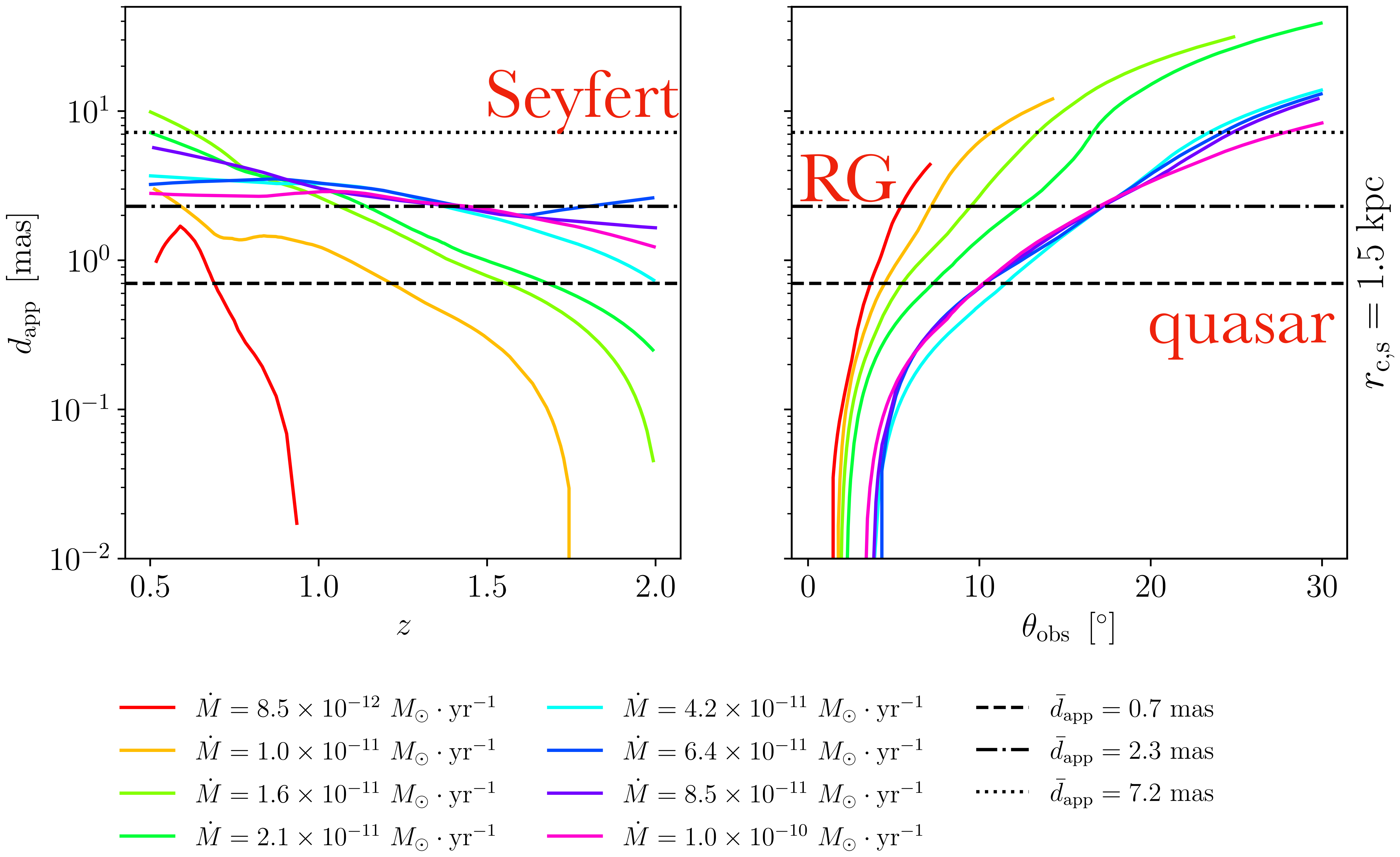

The mass-loading scenario: implications

Observational biases: Doopler boosting plays a major role in regards of the flux selection criteria.

Source type: quasars tends to show near-to-zero offset, observed at low θ_{obs} and higher z, while radio-galaxies and Seyfert at higher θ_{obs} and lower z.

Jet power: Based on optical observations, the offset appears as a unique tool to constraint the jet power.

Gamma-ray emission: Jet-star interactions are often listed to explain gamma-ray emission in jetted AGN (Torres et al. 2019) and in the production of very-energetic cosmic rays (Wykes et al. 2014).

Poster of Bruno Longo
Parsec-scale simulations of jet-star interaction : dynamical and radiative effects

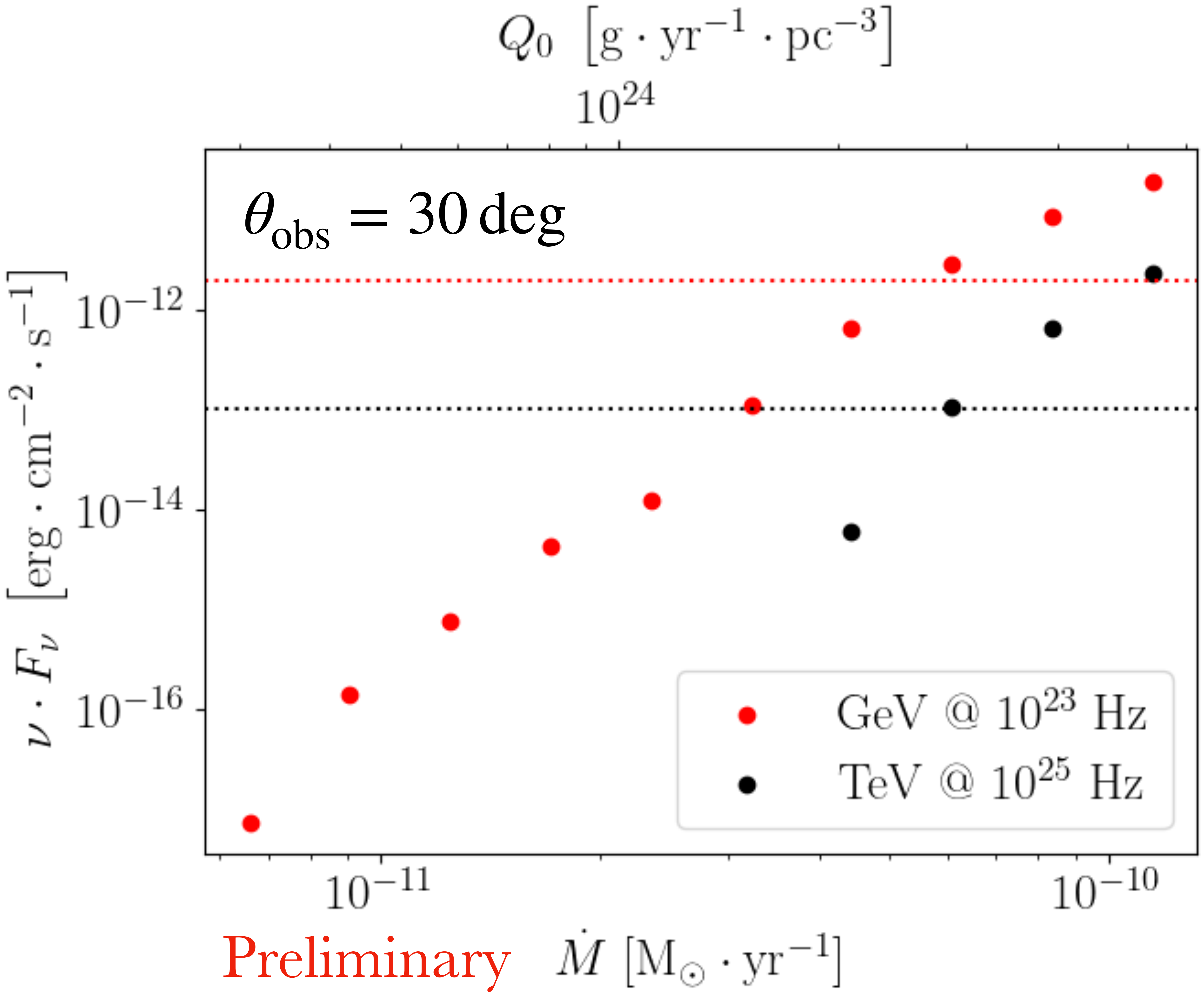

Preliminary

Conclusion and prospects

Jet dynamics and offsets: Mass-loading from stellar winds influences jet deceleration and creates radio-optical offsets; these offsets are useful for probing galaxy properties.

Influence of stellar populations: The presence and distribution of K/M-type stars in host galaxies affect jet emissions and offsets, providing insights into the average stellar mass-loss rates.

Observational implications: Offsets and jet emissions vary with redshift, observation angle, and jet power, which could inform future observational strategies to study AGN jets and their environments.

Observational evidences: Promising qualitative comparison with work of Plavin et al. 2019 underlines the powerful use of radio-optical offset to study AGN.

Conclusion and prospects

Jet dynamics and offsets: Mass-loading from stellar winds influences jet deceleration and creates radio-optical offsets; these offsets are useful for probing galaxy properties.

Influence of stellar populations: The presence and distribution of K/M-type stars in host galaxies affect jet emissions and offsets, providing insights into the average stellar mass-loss rates.

Observational implications: Offsets and jet emissions vary with redshift, observation angle, and jet power, which could inform future observational strategies to study AGN jets and their environments.

Observational evidences: Promising qualitative comparison with work of Plavin et al. 2019 underlines the powerful use of radio-optical offset to study AGN.

Current status: Paper *Jet-Star Interactions: Shedding Lights into Galaxy Properties* submitted for publication.

Conclusion and prospects

Current status: Paper *Jet-Star Interactions: Shedding Lights into Galaxy Properties* submitted for publication.

Jet dynamics and offsets: Mass-loading from stellar winds influences jet deceleration and creates radio-optical offsets; these offsets are useful for probing galaxy properties.

Influence of stellar populations: The presence and distribution of K/M-type stars in host galaxies affect jet emissions and offsets, providing insights into the average stellar mass-loss rates.

Observational implications: Offsets and jet emissions vary with redshift, observation angle, and jet power, which could inform future observational strategies to study AGN jets and their environments.

Observational evidences: Promising qualitative comparison with work of Plavin et al. 2019 underlines the powerful use of radio-optical offset to study AGN.

Jet power: Study the presence and characteristics of radio-optical offsets for a range of jet power.

More refine set-up: inclusion of radiative cooling, presence of accretion disk, stellar population, etc.

Direct comparison: Apply instrumental effects (*Gaia* angular resolution) to directly apply our model to a set of sources showing offsets.

High-energy emission: derivation of high and very-high energy emission in the light of future observatories (CTA).

VNIVERSITAT DE VALÈNCIA

GENERALITAT VALENCIANA

MINISTERIO DE CIENCIA, INNOVACIÓN Y UNIVERSIDADES

Funded by the European Union NextGenerationEU

Max-Planck-Institut für Radioastronomie

γ 2024
8th Heidelberg International Symposium on High Energy Gamma Ray Astronomy
Milano, 2-6 September 2024

Thank you for your attention!

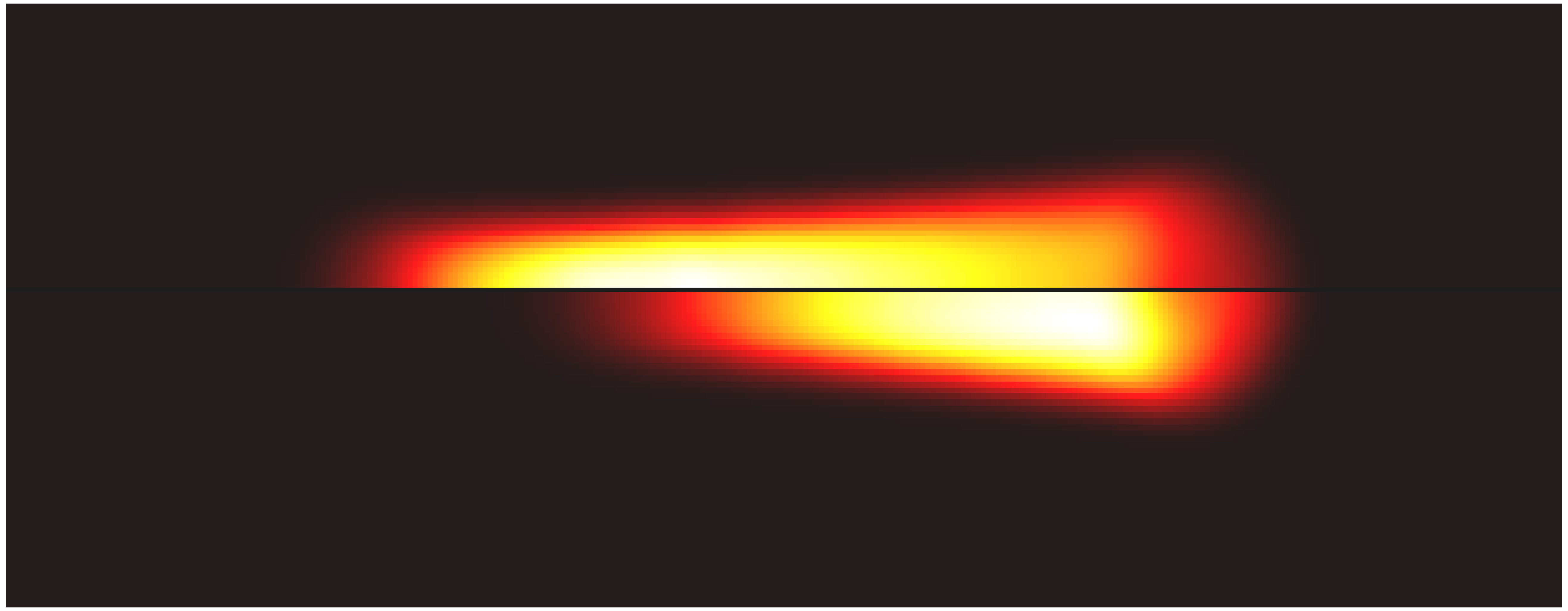

Gaëtan Fichet de Clairfontaine* in collaboration with Manel Perucho, José-María Martí and Yuri Kovalev.

*gaetan.fichet@uv.es

3rd Sept. 2024

References

Anglés-Castillo, A., Perucho, M., Martí, J. M., & Laing, R. A. 2021, MNRAS, 500, 1512

Fichet de Clairfontaine, G., Meliani, Z., & Zech, A. 2022, A&A, 661, A54

Fichet de Clairfontaine, G., Meliani, Z., Zech, A., & Hervet, O. 2021, A&A, 647, A77

Gaia Collaboration, Brown, A. G. A., Vallenari, A., et al. 2021, A&A, 649, A1,

Komissarov, S. S., Porth, O., & Lyutikov, M. 2015, CAC, 2, 9

Perucho, M., Martí, J. M., Laing, R. A., & Hardee, P. E. 2014, MNRAS, 441, 1488

Plavin, A. V., Kovalev, Y. Y., & Petrov, L. Y. 2019, ApJ, 871, 143

Ó Fionnagáin, D., Vidotto, A. A., Petit, P., et al. 2020, MNRAS, 500, 3438